ENVIRONMENTAL RADIATION EXPOSURE HAZARD ASSOCIATED WITH COAL DEPOSITS OF MUI BASIN BLOCK C, KITUI COUNTY

STEPHEN OCHIENG KABASA, (BSC.HONS)

A thesis submitted in partial fulfillment of the requirements for the award of MSc degree in Nuclear Science, University of Nairobi

DECLARATION

This thesis is my original work and has not been presented for the award of a degree to other university

Kabasa Stephen Ochieng'
S56/72370/2011

Signature…… Date……

This thesis has been submitted for examination with our approval as University of Nairobi supervisors:

1) Mr. Michael J. Mangala
Institute of Nuclear Science and Technology
University of Nairobi

Signature…… Date……

2) Prof Eliud M. Mathu
Department of Geological Sciences
Institute of Mining and Mineral Processing
South Eastern Kenya University

Signature…… Date……

ACKNOWLEDGEMENTS

I wish to extend my gratitude to Mr. David M. Maina, Director Institute of Nuclear Science and Technology for his consistent efforts to facilitate the completion of the Master's program; the administrative staff of the Institute of Nuclear Science and Technology for making available the resources used in this study; and Mr. Simon Bartilol, the Senior Technologist for his invaluable contributions during Gamma Spectroscopy analysis.

I thank my supervisors Mr. Michael J. Mangala, Institute of Nuclear Science and Technology, University of Nairobi and Prof. Eliud Mathu, South Eastern Kenya University for their advice and directions to successful completion of my thesis research.

I also thank the National Commission for Science, Technology and Innovation (NACOSTI) for the financial research grant offered to me to facilitate the completion of my thesis research studies. I also extend my appreciation to Mr. John Omenge, the Chief Geologist, Ministry of Energy for availing his staff and vehicles during the field sampling exercise.

I thank the almighty God for the far that he has brought me in completing the MSc Nuclear Science degree program. Lastly, I also extend my gratitude to my parents Mr. and Mrs. Kabasa and my immediate and extended family members for the material and psychological support offered to me in pursuit of my academic endeavors.

LIST OF ABBREVIATIONS

AEDE: Annual Effective Dose Equivalent

D: Absorbed Dose

DL: Detection Limit

H_{ex} and $H_{in:}$ External and internal hazard indices

HpGe: Hyper Pure Germanium

IAEA: International Atomic Energy Agency

NORM: Naturally Occurring Radioactive Material

TGR: Terrestrial Gamma Radiation

UNSCEAR: United Nations Scientific Committee on the Effects of Atomic Radiation

ABSTRACT

Coal is extensively used in the generation of energy, the byproducts of which have profound applications in the building and construction industry and in agriculture. It is no doubt that the exploitation of coal deposits in Kenya will spur the development of infrastructure, create employment and significantly influence the socio-economic structure. However, the mining process also has its negative effects to the environment, and the public in general; such as radiation exposure.

In general, living organisms are continuously exposed to cosmic and other terrestrial ionizing radiation. However, exposures vary between localities due to altitude and geological characteristics. Other human activities also contribute to increased exposures to ionizing radiation. These include; metals mining, coal fired power plants, phosphate rock mining and their subsequent use in fertilizers, natural gas production, gas mantles, luminescent dials, medical diagnostics and treatment, industrial radiography and air travel are some of the activities that significantly modify the environmental exposure to ionizing radiation. In general, coal excavation among other mining activities tend to increase the risk of exposure to harmful gamma radiation. Studies on exposures to high radioactivity levels indicate detrimental effects.

The aim of this study therefore, was to assess the radiation hazard risks associated to the coal deposit in the Mui Basin Block C prior to the start of mining activities. This study evaluated the radiation levels in soil samples from Yoonye, Kathonzweni and Kateiko within the coal rich block C that covers approximately 131.5 km^2 of the Mui basin in Kitui County. Specifically, the study was undertaken to evaluate the background radiation levels and radionuclide concentration levels in these areas. Forty-two (42) soil samples were collected between 19th and 22nd August 2013 from Block C at between 10 to 20 cm depth for gamma spectroscopy analysis. The samples were crushed, sieved, weighed and stored in plastic sealed containers for 21 days before counting was performed.

Radionuclide activity analysis was done using gamma-ray spectrometer HpGe detector Model No. CPVD530-30185 SN 2489 with a 30% efficiency, 1.8 KeV (FWHM) resolution at 1.33 MeV peak of Co-60 and MAESTRO PC based software for analysis of the spectral data. The activity concentration of ^{232}Th was found to be between 9.7±5.6

and 130±5 Bqkg^{-1}, ^{238}U was between 14. 2 ± 2.9 and 75. 9 ± 4.2 Bqkg^{-1} and ^{40}K was between 348±18 and 1678 ±73 Bqkg^{-1}. More than 80% of the soil samples measured in this study had activity concentrations higher than the reported world average values of 30, 35 and 300 Bqkg^{-1} for ^{238}U, ^{232}Th and ^{40}K respectively. The gamma absorbed dose was found to be between 48 and 173 nGyhr^{-1} with more than 90% of the soils sampled having values exceeding the estimated world absorbed dose average of 60nGyhr^{-1}. The radium equivalent dose was determined to range between 98.31 and 344 Bqkg^{-1}which is below the ICRP recommended threshold value of 370 Bqkg^{-1}. The internal hazard index ranged from 0.32 to 1.14 whereas the external exposure hazard indices ranged between 0.27 to 0.96. About 4 soil samples from the sampled region had internal hazard indices above unity.

There were no statistically significant differences in ^{232}Th and ^{238}U activity concentrations of soils sampled from Yoonye and Kathonzweni (p^{232}_{Th} = 0.821, p^{238}U = 0.937), Yoonye and Kateiko (p^{232}Th =0.86, p^{238}U = 0.53), Kateiko and Kathonzweni (p^{232}Th = 0.76, p^{238}U = 0.42) all at $p< 0.05$ respectively. However, there were significant differences in the ^{40}K activity concentration levels between soil samples from Yoonye and Kathonzweni ($p = 0.026$) at $p<0.05$. In general, soil samples from Yoonye had much higher ^{40}K activity concentration compared to those from Kathonzweni and Kateiko.

In regard to the radiation exposure hazard indices and radium equivalent, the absorbed dose and the annual effective dose equivalent, the difference was not significant at $p<0.05$.

In summary, the study has enabled determination of the radioactivity levels in Block C of the Mui Basin whose levels currently do not pose radiation health hazard risk.

CONTENTS

LIST OF FIGURES

LIST OF TABLES

CHAPTER 1

INTRODUCTION

1.1. Background

High natural background radiation due to anomalous concentrations of primordial radionuclides have been reported in Yang Jian China (Mohantya et al., 2004), Ramsar Iran, Guarrapari and Minas Gerias Brazil (Ramli et al., 2009), Abeokuta and Jos City Nigeria (Farai & Jibri 2000) not forgetting to mention, Usaki near Homa bay in south Nyanza, Mrima Hills along the Kenyan South Coast, and Ruri and Homa mountains in western Kenya (Mustapha et al., 1997).

Weathered carbonatite rocks containing high concentration of thorium, have been reported to contribute to the absorbed dose ranging between $200nGyh^{-1}$ to $14000nGyh^{-1}$ measured in Mrima Hills (Patel 1991). The presence of monazite sands, volcanic intrusion, high potassium concentrations due to potassium bearing minerals; biotite, muscovite, orthoclase, microcline, feldspars, radioactive minerals; smectite, kaolite, uranium minerals (uraninite, sphene, monazite, zircon and zircon containing heavy sands) are the cause for the high background radiation levels (Okeyode & Ganiyu, 2009).

From these studies, it is evident that mineral deposits and the composition of the underlying rocks contribute significantly to the radioactivity levels of a particular area. In addition, areas located at high altitudes tend to have higher radiation levels. Economic activities such as mining, building and construction, agriculture among others have been known to contribute to high radiation levels of a particular area (UNSCEAR, 2008).

Inhabitants of high background radiation areas (HBRAs) are susceptible to prolonged exposure to abnormally high radiation levels over successive generations (Al Safarjalani, Al-Dakheel & El Mahmoudi, 2007). The elevated background ionizing radiation may pose detrimental side effects such as somatic and genetic effects that may damage critical and radiosensitive organs and eventually lead to death. Cosmic rays in the atmosphere and natural radionuclides in air, food and drinking water contribute majorly to radiation exposure through inhalation and ingestion.

Natural radionuclides are categorized into three major decay series; the thorium series (4n), the uranium/radium series (4n+2) and the actinium series (4n+3). In addition, there is a fourth series, (4n+1) of artificial radionuclides. In general, each series undergoes sequential transformations that start with a long lived parent radionuclide and ends with a stable nuclide. Figure 1-1 shows decay series chains for the ^{238}U and ^{232}Th series which has 14 and 10 nuclei respectively, that terminate to stable ^{206}Pb and ^{208}Pb.

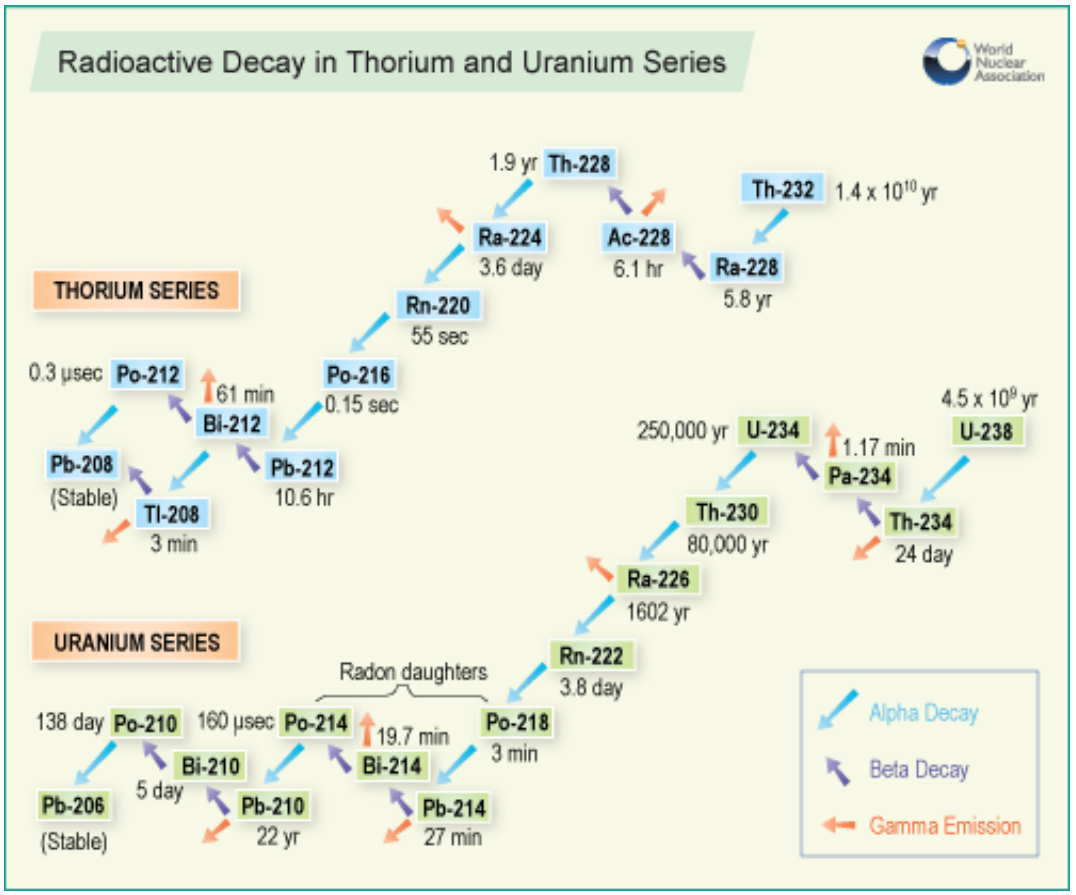

Figure 1-1: Uranium and Thorium decay series (IAEA 2003)

Other radionuclides that do not belong to any of the above series and are long-lived include; ^{14}C, ^{40}K, ^{50}V, ^{87}Rb, ^{115}In, ^{130}Te, ^{138}Ln, ^{142}Ce, ^{114}Nd, ^{147}Sm, ^{176}Lu, ^{187}Re and ^{192}Pt. The abundance in the Earth's surface of ^{40}K makes it of radiological importance.

In general, environmental radioactivity contamination assessment of a given area relies on the evaluation of natural radionuclide distribution in the soil, water and in air. Natural radionuclides of the uranium series, thorium series and their decay progeny's and also potassium (^{40}K) have been identified as the major source of measurable natural ionizing radiation with significant contribution to the environmental gamma radiation

exposure dose. It is estimated that terrestrial radiations from natural radioactive elements originating in the ground, stones, trees, and the walls of buildings contribute on the average about 0.28 $mSvy^{-1}$ (IAEA, 2002).

Coal is formed through the subjection of organic matter to intense heat and pressure over millions of years. Coal is conventionally extracted through surface and underground mining. Globally, coal production and consumption has been estimated at seven billion metric tons in 2009; of which, 44% has its origin in China, 14% from the United States and 8% from India (Muthangya & Samoei, 2006). Coal has been shown to contain ^{238}U and ^{232}Th, as well as their decay products and ^{40}K radionuclides (Životić et al., 2008). In general, the total levels of individual radionuclides in soils are typically the same as those found in underlying rocks in the coal deposit area. This contributes to the variation in the distribution of radionuclides based on region and geology and their enhancement due to presence of other heavy metals and high sulfur content (IAEA 2003). The combustion of coal produces coal combustion residues (CCRs); carbon dioxide (CO_2), sulphur oxides (SOx), nitrogen oxides (NOx), chloro flouro carbons (CFCs), other trace gases and air borne inorganic particulates, such as fly ash and suspended particulate matter (SPM). Carbon dioxide, nitrogen oxides and chloro fluoro carbons are greenhouse gases (GHGs) which affect the environments general aesthetics such as land use, air, soil and water thereby leading to environmental pollution (Vatalis & Kaliampakos, 2006).

The contents of radionuclides in bottom ash and flyash can be in excess of ten times or greater than coal. Flyash is often used in building construction industries; bricks making, cement manufacturing, ceramics, and in agriculture; fertilizers which facilitates nutrient uptake and improves vegetation growth. (Shamshad, Fulekar & Bhawana, 2012; Senapati, 2011: Mukherjee & Vesmawala, 2013). Therefore, the implications of Coal mining and the subsequent applications of byproducts as a potential naturally occurring radioactive material (NORM) intensifiers is a matter of concern for radiation protection purposes.

Open pits or underground mines are the conventional techniques of coal mining which can result in significant amounts of waste with elevated levels of radionuclide concentrations (Sleziak et al, 2010). Underground coal mines, mining waste rocks and soils may have elevated radon, radium and ^{40}K levels. Waste water from coal mines

have been measured with activities of between and 15,000 $Bqkg^{-1}$ to 55,000 $Bqkg^{-1}$ (IAEA 2003).

Moreover, toxic elements such as arsenic and mercury as well as ^{226}Ra and ^{228}Ra were found in coal ash following a coal spill at the Tennessee Valley Authority (TVA) coal-burning power plant in Kingston, United States on December 22, 2008. The release of these substances into the environment poses a health risk to local communities due to their potential to be resuspended in the ambient atmosphere (Ruhl et al. 2009).

Coal-fired power stations, compared against the nuclear fuel cycle is believed to release more radionuclides into the environment (IAEA 2003). However, flue gas desulphurization, emission reduction technology; scrubbers and filters aim to reduce emissions within acceptable levels. However, these technologies are only effective with large particulates.

Despite the anticipated wealth and employment opportunities that the coal presents, the extent of adverse influence on traditional values and environmental degradation once mining begins cannot be overlooked. The introduction of mining activities will increase radiation exposure to terrestrial gamma radiation and monitoring the radioactivity levels will be essential in the management of radiation exposure. Using the derived activity concentration of various radionuclides present in soil samples, the radiation exposure parameters; absorbed dose, annual effective dose are determined for compliance with the ICRP recommended limits. This study presents the opportunity to determine the baseline data for the distribution of radionuclides in the environment prior to the commencement of coal mining and extraction activities in the area

1.2. Scope of the study

Soil and other building materials have natural radioactivity that results in internal and external radiation exposure (Frissel 1994; Ahmad et al. 1997; Ibrahim, 1999). Outdoor exposure is due to the natural terrestrial radiation that emanates primarily from the subsoil 30 cm deep (Ramli et al., 2009).

Specifically, this study is limited to the assessment of gamma radiation exposure from naturally occurring radionuclide of ^{238}U, ^{232}Th, their decay progenies and ^{40}K in the soil samples from the coal deposit area of Block C, Mui Basin Kitui County. Gamma

spectroscopy method was used to analyze soil samples for the activity concentrations of ^{238}U, ^{232}Th and ^{40}K.

1.3. Problem Statement

Coal mining has been identified as a major source with significant contributions to the increase of Naturally Occurring Radioactive Material (NORM) into the environment. Coal contains ^{238}U, ^{232}Th as well as their decay progeny and ^{40}K. Approximately 10,000 tons of Uranium and 25,000tons of Thorium are produced annually from coal fired power plants worldwide. In addition, the estimated radioactivity of the earth's crust is $1400Bqkg^{-1}$ which is indicative of high radioactivity levels in the earth that can be released into the environment following mining activities (IAEA, 2003).

Studies conducted in other countries; Poland, Australia, and China show significant coal radionuclide content (IAEA, 2003). The waste rock and soil material, drainage water and also the coal itself may pose a risk of radiation exposure (Sleziak et al., 2010). A strong correlation has been shown to exist between the underlying rock radionuclide concentrations and soil radionuclide concentration and distribution, enabling the evaluation of the radiation exposure hazard risk in certain areas (Okedeyi et al., 2012).

This study will pioneer subsequent investigative studies for evaluation of radiation exposure levels associated to natural background radiation in Mui Basin (Block C) prior to the commencement of coal mining activities and for future environmental radiation monitoring program.

1.4. Objectives of the Study

1.4.1. Broad Objective

To assess the environmental radiation exposure hazard from soil samples associated with coal deposits of Block C, Mui Basin prior to commencement of mining activities.

1.4.2. Specific objectives

1) To measure the activity concentrations of the natural radionuclides ^{238}U, ^{232}Th and ^{40}K in the soil samples from Block C, Mui basin, Kitui County using HpGe gamma ray spectroscopy analysis;

2) To assess the radiation exposure hazard associated to gamma radiation exposure in Block C of the Mui Basin by estimating the gamma absorbed dose rate, the annual effective dose equivalent and the internal and external hazard indices

1.5. Justification and Significance of the Study

Most natural materials contain radioactive elements such as ^{238}U, ^{232}Th and ^{40}K. Mineral sands, titanium and zircons have been shown to contain significant radionuclide levels. Monazites and rare earths containing thorium as well as other elements of economic importance have been shown to have substantial radioactivity.

Naturally occurring radionuclides; ^{238}U, ^{232}Th and ^{40}K are long lived and are present in the soils in varying amounts depending on the origins of the parent rock and the underlying geology. Secondary radionuclides are also radiogenic and are derived from the decay of primordial radionuclides or are continuously formed in the environment from interactions of cosmic rays.

In general, the decay of these radionuclides may cause harmful effects due to the resulting ionizing radiation exposure such as cell damage among other abnormalities. The radiation exposure hazard risk associated to use of soils as building materials has not been evaluated in the study area. The purpose of this study is therefore relevant for;

1) Radiation protection and safety for the general public and workers;
2) Study of the distribution of natural radionuclides in the soil samples associated to coal deposits in the block C Mui basin for comparison to other studies elsewhere;
3) baseline data on radioactivity contamination prior to mining activities in the study area for future environmental impact assessment evaluation and therefore sensitize the local community and stakeholders on possible health impacts.

CHAPTER 2

LITERATURE REVIEW

2.1. Introduction

The radioactive decay of ^{238}U, ^{232}Th and ^{40}K significantly contribute to exposure through ingestion and inhalation (Walter, David & Glen, 2006: IAEA 2003: IAEA 2002). The earth's crust contains approximately 10 and 14 parts per billion of thorium and uranium respectively. In general, approximately 70 naturally occurring radionuclides belonging to the natural decay chains/series are known in addition to several light radioactive isotopes.

2.2. Sources and Mechanisms of Exposure to Ionizing Radiation

Exposure to terrestrial gamma radiation depends on the type of the soil, geological features and geographical conditions (UNSCEAR, 2000; Olarinoye et al., 2010). Radionuclides become incorporated into the rock in the early rock formation stages and are released into the soil during the rock cycle stages of weathering (Gessel & Prichard, 1975; Florou & Kritidis, 1992). In general, higher levels of radionuclide concentrations are associated with igneous rocks such as granite whereas sedimentary rocks have lower levels (UNSCEAR, 2000).

In the uranium decay series, ^{226}Ra and its daughter ^{222}Rn are of special interest; specifically, ^{226}Ra is responsible for major radiation dose received from internal exposure mainly because it is present in rocks, water, earth, food and human tissue. ^{226}Ra mimics calcium and is deposited in the bones and may eventually lead to the development of cancer, as was observed in radium watch dial painters. ^{226}Ra decays via gamma ray emission to ^{222}Rn which is a major contributor to radiation exposure approximately 43% (Figure 2-1). Radon exposures have been found to be significant in homes built of granitic soils and materials. Short-lived decay products of radon are retained for long in the lungs after inhalation. The indoor radon related dose is approximated at 2mSv/yr (Mohankumari, Anandaram, & Shilpa, 2014).

^{40}K is a predominant radioactive β- emitting component of foods and human tissue and decays with a characteristic 1460 KeV gamma emission. The natural body concentration of ^{40}K contributes approximately 17mrem/y of the whole body dose. The

activity of ^{40}K is approximately 855pCi/g of potassium. Potassium concentration ranges between 1000 and 30,000 ppm in soils but usually much lower and more variable in basaltic rock regions compared to acidic rock regions. Granite rocks are reported to have concentrations of about 29,000 ppm (IAEA, 2002).

Occupational radiation exposures are also significant contributors to dose received by an individual e.g. flight crew and tour guides are exposed are exposed to higher levels of cosmic and radon respectively, whereas miners working with material with high radioactive content are also susceptible to excessive exposure, X ray technicians and workers working in nuclear facilities are at risk of high radiation exposure (Tomza & Lebecka, 1981; Lebecka et al. 1987: Skubacz et al. 1992).

Sources of NORM in the environment have been associated with several activities; such as the coal mining industry, oil and gas industries, metal mining and smelting, mineral sands, phosphate mining building industry and nuclear fuel recycling (Karangelos et al., 2004). Ingestion and inhalation, present environmental pathways for internal exposures that could lead to a potential health hazard (Turhan & Gunduz, 2007; Petropoulos, Anagnostakis, & Simopoulos, 2002: UNSCEAR 1993).

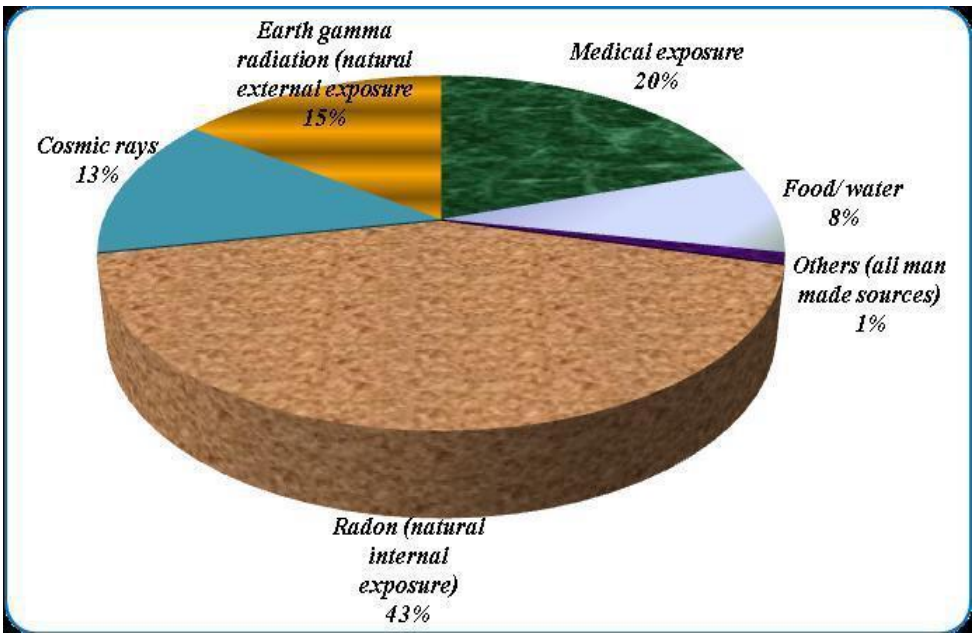

Figure 2-1: Contribution of various sources to dose (IAEA 2003)

In general, the total radiation dose to an individual is a contribution from a variety of sources; natural radionuclides (^{238}U, ^{232}Th, and ^{40}K) contribute 80% and cosmic rays 17%. Uranium contributes the highest dose ≈ 55% and cosmogenic radionuclides

contribute ≈ 1% to total radiation annual effective dose equivalent-AEDE (IAEA 2003: Figure 2-1).

In general, other studies have shown significant concentration of primordial radionuclides, specifically ^{238}U and ^{232}Th in beach sands. Coastal Kalpakkam India, Guarrapari and Minas Gerias Brazil have been found to have activity concentrations of primordial radionuclides higher than the estimated world averages (Kannan et al. 2002: Ramli et al. 2009: Freitas & Alencar 2004). The activity concentrations of ^{232}Th and ^{238}U in beach sands have been found to range between 36–258 and 352–3872 Bq kg^{-1} respectively. The high radionuclide concentration and high background radiation doses of between 75 to 14,400 nGy h^{-1} have been attributed to monazite in beach sand samples. However, ^{40}K has been found in lower concentrations in beach sands similar to surrounding soils (Kannan et al. 2002).

The high background radiation levels are not only limited to coastal beach sands. The iron ochre region of Um-Greifat, Egypt, are reported to show activity concentrations of 1858 and 4062, 29 and 151, 46 and 409 $Bqkg^{-1}$ for ^{238}U, ^{232}Th, and ^{40}K. Moreover, the corresponding resultant radium equivalent activities (Ra_{eq}), the external and internal hazard indices (H_{ex}, H_{in}) were found to exceed the ICRP permitted values of 370 $Bqkg^{-1}$ and 1, respectively. These results were reported to be indicative of a health risk burden in these areas, where the basement igneous and metamorphic rocks comprised of uraniferous granites, Miocene sediments mostly clastic-carbonates containing ochre with high radionuclide content contribute to the high background radiation (Nada, 2002).

Cement, stone, bricks, and soil commonly used in construction have been found to contain naturally occurring radioactive materials. In studies related to building materials, bricks samples have been found to contain more ^{226}Ra as compared to the other materials such as marble samples. Low ^{232}Th contents were measured in the marble and cement, while sand had intermediate values (Mustapha et al., 1997: Tchokossa, Makon, & Nemba 2012).

Various studies on high background radiation associated to granitic rocks are very common. Cetin, Altisoy & Orgun (2012) determined the concentrations of natural radionuclides in granitic rocks using HpGe gamma-ray spectroscopy. ^{226}Ra and ^{232}Th

were found to range between 0.7± 0.1 and 186 ± 1 $Bqkg^{-1}$, and 0.5 ± 0.1 to 249 ± 2 $Bqkg^{-1}$ respectively. From mineralogical analyses, orthoclase and radiogenic minerals were responsible for the high activity concentration levels.

In Kenya, various areas have been identified as regions of high TGR; Jombo and Mrima Hills in the Mombasa-Kwale area of southern Kenya, Ruri and Homa hills in western Kenya, and Usaki near Homa bay in south Nyanza (Mustapha et al., 1997). Ruri hills and some of the other areas in Lambwe east location of Mbita district, southwestern Kenya, have been shown to have dose rates typical of worldwide high background radiation areas with mean absorbed dose rates 40 times the global average. The enhanced level of background radiation in the western Kenya study area was attributed to^{232}Th in carbonatite rocks (Achola et al. 2012).

The Tabaka region in Kisii is popular for its soap stone quarries. However, gamma absorbed dose rates of 177.6$nGyh^{-1}$; four times higher than the world average of 43$nGyh^{-1}$ have been measured in this area (Kinyua, Atambo, & Ongeri, 2011). In the study, the annual effective dose equivalent (AEDE) was found to correspond to an excess lifetime cancer risk of 0.07%. In the evaluation of the external and internal radiation hazard indices, it was found that, they were all above unity and exceeded the ICRP permissible limits.

The Limestone from regions of Kitui South, adjacent to the Mui basin where the present study was undertaken, have also been studied for radionuclide concentrations; ^{226}Ra, ^{232}Th and ^{40}K. The activity concentration, annual effective dose equivalent, and radiation hazard indices were found to be below recommended radiological safety levels (Mulwa, Maina & Patel 2010). The activity concentration of ^{232}Th was below detection limits whereas, the average activity concentrations for ^{226}Ra varied from 28.3 to 47.4 $BqKg^{-1}$ with a mean value of 35.9 $Bqkg^{-1}$ and 87.4 to 142.6 $BqKg^{-1}$ with an average of 108.5 $BqKg^{-1}$ for ^{40}K. Based on the findings of the study, the limestone from the area was however found suitable for building purposes.

Related to the present study, radionuclides contaminated mine tailings contribute to the spreading of contamination to the surface. Soils and sediment samples associated to coal mining contain radioactive ^{40}K, ^{226}Ra, and ^{232}Th, as well as the anthropogenic radionuclide ^{137}Cs. These have been reported as the most important contributors of Vistula river contamination (Sleziac et al. 2010).

Hassan et al., (2013), studied coal soils and water to determine the natural radioactivity in samples from Barapukuria coal mine, Bangladesh. The values of ^{238}U, ^{232}Th and ^{40}K were reported to be higher than world averages for soil samples. However, the external hazard indices and radium equivalent activity were lower than the world average values.

From these studies it is evident that the terrestrial gamma radiation varies for different geographical areas and is frequently dependent on the geological characteristics of the area.

2.3. Effects of Low Dose Radiation on Health

The BEIR VII (2006) defines low doses as those in the range of near zero up to about 100 mSv (0.1 Sv) of low-LET radiation. However, there are difficulties in attributing specific cases of diseases to low dose radiation exposures. The lack of specificity in type and characteristic of disease induced by radiation exposure, the long delay between exposure and disease presentation and the high spontaneity in incidences of diseases associated with radiation in ageing of the general population are confounding factors in assessing health hazards due to exposures from radiation at low doses. Therefore, no substantial evidence links low dose radiation exposure to increased incidences of cataracts or elevated incidence of circulatory disease as observed in populations irradiated at high radiation dose exposures (IAEA 2002).

2.3.1. Cancer Incidence

Epidemiological evidence shows that exposure to ionizing radiation at low, moderate and high levels can lead to excess incidence of tumors in body organs. However, cancers are due to many causes and frequently severe in humans at advanced stages of development. Epidemiological and mechanistic studies are used to assess radiation health effects (BEIR VII 2006: IAEA 2002: Gahrouei 2003). However, increase in cancer incidences due to radiation exposure is modest.

Some studies have shown no significant correlation between cancer mortality and the cumulative dose (Tao, Cha & Sun 1999). Moreover, these studies show a reduction in incidence of cancer at low background radiation (Gahrouei, 2003; Toshiyasu, 2009: Cuttler & Pollycove, 2009: Karam, 2002).

On the other hand, other studies suggest that about 20% by proportion of childhood leukemia in Great Britain is induced by natural background radiation (Wakeford,

Kendall, & Little, 2009), with fetuses being more susceptible to radiation than adults (Akiba, 2000).

2.3.2. Non Cancer Diseases and Anomalies

The relationship between irradiation at low doses of between 1Sv to 2Sv and radiation associated non- cancer diseases has not been clearly defined. However, emerging evidence indicates increased incidence of non-cancer diseases between doses 1-2 Gy and even lower. Apart from the deterministic effects of exposure to certain radiation levels, stochastic effects are more problematic to ascertain (UNSCEAR, 2008).

2.3.2.1. Radiation and Cell Mutation

Heritable effects due to radiation exposure originate from damage to DNA of germ cells in reproductive organs. Mutations are then passed on to offspring's and future generations. The mutation may become dominant and eventually lead to dominantly inherited diseases or indirectly produce chronic multi-factorial diseases. These diseases contribute to congenital disorders in children (IAEA, 2002).

Studies have shown no significant effect on the induction of spontaneous micro-nuclei in newborns or any change in length of telomeres in adults as a result of exposure to low background radiation (Das, 2010). In contrast, significantly reduced chromosomal aberrations have been reported in inhabitants of high background radiation areas of Iran (Ghassi-Nejad et al., 2004; Karam, 2002).

Other studies suggest adaptive responses are induced by chronic exposure as opposed to acute exposures. These adaptive responses are referred to as Radiation Hormesis discussed elsewhere in this study. In addition, immune systems and hematological alterations have shown no differences in people living in high and low background radiation areas (Cuttler & Pollycove, 2009).

2.3.2.2. Radiation Exposure and Trace Metal Levels in Humans

The role of trace metals in the human body is important for vital processes that maintain physiological functions of the body. Changes in the concentrations of these elements cause serious changes in physiological activities. Researchers and medical practitioners measure these elements as parameters in the study of chronic effects of radiations.

High natural background radiation areas are believed to have an effect on the concentration of Cu, Zn, Fe and Mg in the blood. Radiation workers has been found to have lower Cu and Mg. However, the concentration of iron and zinc were found to be higher in radiation workers (Shahbazi-Gahrouei & Abdolahi, 2012).

Chatterjee et al. (1994) reported a significant increase in the concentration of Cu, Fe and Zn in the hair of X-ray technicians. Moreover, the study supports other studies that show the levels of Cu and Zn in blood to be depleted as Fe level is increased. From the studies, sex of study group influenced concentration of the metals in the blood (Ebrahiminia et al., 2008; Cengiz et al., 2003).

2.3.2.3. Radiation Hormesis

The induction or activation of cellular protective capacity is also proposed to be a likely effect of radiation exposure (Boreham et al., 2006). Radiation Hormesis refers to irradiation with enhancement of protective capacity which predominates over detrimental effects at low levels of radiation exposure with beneficial net health consequences. Cuttler & Pollycove (2009) reports that ionizing radiation at low dose rates have stimulatory rather than inhibitory effects. In general, exposure to ionizing radiation may have epidemiological implications (IAEA 2002; Roger & Beverly, 1991).

In the 1930s, radium was considered a vital entity in producing profound feats of rejuvenation; mild radium therapy treatments were administered at microgram levels. ^{226}Ra and ^{228}Ra were used to treat metabolic diseases, diabetes, hypertension, infertility and impotence. Unlike oncology that utilizes high doses that may be destructive, mild radium therapy utilized small amounts (Roger & Beverly, 1991).

Various hormetic effects of radiation exposure have been proposed and include; DNA repair (IAEA 2002: Ghassi-Nejad et al., 2004), free radical detoxification and repair system (Cuttler & Pollycove 2009), immuno-stimulant effects (Roger & Beverly 1991), metabolic catalyst and fertilizer enhancement. Luckey (2008) alluded that life forms that are deprived of ionizing radiation are likely to show deleterious effects. He further resolved that, optimal organism proliferation occurred in the presence of baseline ionizing radiation and that doses that are substantially above and below this optimal radiation level could result in suboptimal growth.

Radiation deficiency syndrome refers to incidence of low growth rates, receding of development, reduction in fecundity, deteriorating health, slow metabolism and short lifespan that could result from lack of ionizing radiation. However, there are no conclusive data to support these conditions. The selective inactivation of senescent or inhibiting structures in plants and higher organism, lifespan extension capability and low level radiation as an evolutionary driver are some of the effects that have also been proposed (Cuttler & Pollycove 2009).

2.3.3. Radioactivity in Food Crops Grown High Background Radiation Areas

The uptake of essential minerals, in both edible and inedible parts of plants is dependent on the types of soils, the mineral concentrations, and bio-availability. Processes within the plants biological mechanism make the nutrients available for ingestion and therefore lead to exposure (Shanthi et al., 2009). Soil additives such as fertilizers; especially phosphate based fertilizers, contain high uranium content, which is likely to contribute to elevated levels in vegetables grown with these fertilizers (Ahmed & El Arabi, 2005; Saleh et al., 2007: Harb S et al 2008).

In general, the concentration of the natural radioactivity in food crops range between 40 and 600 Becquerel per kilogram. Ramachandran and Mishra (IAEA 2002) reported concentration of radionuclides in various foods; ^{40}K was reported to range between 45.9 and 649.0 Bq/kg, ^{226}Ra between 0.01 and 1.16 Bq/kg and ^{228}Th between 0.02 and 1.26 Bq/kg. The bioavailability of radionuclides is dependent on the availability of radionuclides in food stuffs (Frissel 1994). In comparison to the soil radionuclide content, the corresponding concentration in plants is significantly low.

Plants grown in low background radiation areas are reported to have negligible radionuclide concentrations. However, ^{232}Th has been shown to be higher in foods compared to ^{226}Ra and ^{238}U. This is as a result of ingrowth of ^{228}Th from ^{228}Ra and ^{228}Ac that is taken up by plants (Shanthi et al. 2009).

It is known that potassium is an essential macronutrient that is required and bio-available to plants in high quantities. Soil characteristics will more likely favor the mobilization of potassium and its consequent translocation into plants. The fact that potassium is an important nutrient makes its content in the body a physiological characteristic rather than an intake property. ^{40}K is homeostatically controlled in human

cells. The high consumption of rice as a staple food is a likely explanation for high radioisotope concentrations. Some plants and foods have been shown to have much higher radionuclide concentrations than others (Shanthi et al. 2009).

Following the foregoing deliberations on the effects of low dose radiation on human, and plants, it is clear that radiation in whatever level, has continued to elicit interest. The measurement of radiation exposure is fundamental to environmental radiation protection. In Chapter 3, we discuss the basic principles of radioactivity measurements.

CHAPTER 3

RADIOACTIVITY AND GAMMA RAY MEASUREMENT

3.1. Historical Background

Wilhelm Roentgen in 1895 first observed fluorescence emitted from a glass Hittorf-Crookes tube while studying cathode rays. The invisible rays were found to penetrate opaque black paper and Roentgen referred to them as X rays. Henri Becquerel later followed suit in investigating these supposedly mysterious rays, choosing instead to work with potassium uranyl sulfate. The uranium was found to affect photographic paper, even when wrapped in black paper, and this marked the discovery of spontaneous emission of radiation by matter. The emitted radiation was found to have a close semblance to *X* radiation.

Marie and Pierre Curie later discovered that, apart from uranium's spontaneous disintegrations, there existed other elements that exhibited a similar property. These discoveries led to use of the term radioactivity. Ernest Rutherford elaborated many concepts referring to the atom and radioactivity. He discovered that aside from electromagnetic rays, radioactive material also emitted particles that he later characterized and named alpha (α) and the beta (β^{-}) particles.

Ernest Rutherford, Hans Geiger and Ernst Marsden in 1911, experimentally proved wrong the earlier Thomson's theory of matter, that electrons were randomly dispersed in the atom. By bombarding a thin gold foil, with a beam of *alpha* particles, they observed that most of the particles passed through the gold foil un-deflected, others were deflected at divergent angles, while some bounced back contrary to Thomson's theory of matter, in which the *alpha* particles would be deflected uniformly

The difference observed between Thomson's expected scattering cross section and Rutherford's experiment, led Rutherford to suggest a new atomic model. According to his model, the positive charges were concentrated in a very small nucleus where most of the atomic mass was (99.95%) and the electrons orbit around the nucleus in the same way as a planetary system. Based on this theory, the positively charged *alpha* particles were deflected by the positive nucleus, through Coulomb electric repulsion. The closer they passed to the nucleus the more deflection, up to a point they are pushed back from a direct hit with the nucleus hence the observed bouncing back.

Niels Bohr drawing on Rutherford's experiment, proposed an atomic model free of the drawbacks of the planetary model that could not explain why atoms emit electromagnetic waves of certain frequencies only, and why a moving charged particle, like the orbiting electrons, does not continuously radiate electromagnetic energy. According to Bohr's atomic model, electrons rotate around the nucleus along fixed predefined orbits and therefore the classical theory of electromagnetic emission no longer applied. These theories and postulates are the backbone upon which current developments in Quantum Mechanics are derived.

Radioactivity is a property of some atomic nuclei to spontaneously disintegrate thereby emitting highly energetic particles (α and β^- radiation) or electromagnetic radiation (γ radiation) as key signatures of nuclei disintegration. Knowledge about the atom and the nucleus has developed significantly following the discovery of radioactivity. The disintegration process of an unstable nucleus is stochastic, therefore a system of many nuclei must be considered.

The average number of disintegration or activity of the system, N, per time interval, t, is related to the mean lifetime of a nucleus and the number of unstable nuclei in the system by $N = N_0 e^{-\lambda t}$, where, λ is the decay constant.

The nucleons are bound together by the strong nuclear interaction force. The strong nuclear interaction acts on nucleons that get close enough to each other, and is independent of their mass, size, structure, and electrical charge. When the distance between particles is less than a few femtometers (fm = 10^{-15}m), typical of the nucleus, the nuclear interaction develops a strong attraction between the particles. The repulsive Coulomb interaction between charged predominates at distances greater than this.

The binding process lowers the energy level of each nucleon and from the theory of relativity; the negative binding energy between the nucleons generates a decrease in the total mass, $\Delta E = mc^2$. The binding energy of a nucleus is dependent on the number of nucleons present. The binding energy per nucleon increases rapidly for nuclei with few nucleons and saturates for nuclei with ≈60 nucleons (Figure 2-2).

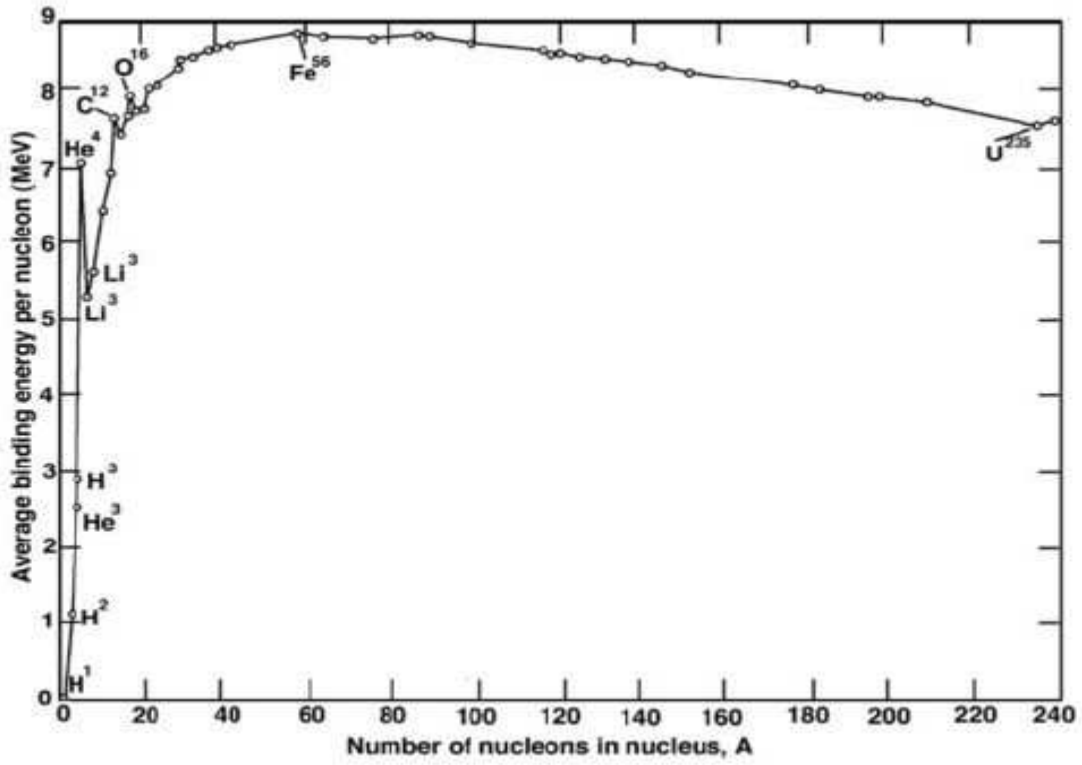

Figure 3-1: Plot of the average binding energy per Nucleon of various nuclei (Walter, David & Glen 2006)

The energy per nucleon for heavier nuclei decreases almost constantly. The decrease in the binding energy can be attributed to the very short range of the strong nuclear interaction (≈2 fm) in addition to the Coulomb interaction between protons. The strong nuclear interaction of heavy nucleus decreases as a result of the core size; the core size is bigger than the interaction range. Moreover, an increase in the Coulomb interaction between protons destabilizes the core. In general, nuclear behavior is explained by several models and theories in certain circumstances.

The stability and the binding energy of nuclei is well explained by the liquid drop model. The nucleus in this instance is regarded to be sphere with uniform interior density, like a drop of liquid. The semi-empirical equation based on the model has been used to estimate the binding energy of a nucleus.

$$E_{Z,A} = f_0(Z,A) + f_1(Z,A) + f_2(Z,A) + f_3(Z,A) + f_4(Z,A) + f_5(Z,A) \quad \ldots\ldots\ldots\ldots\ldots\ldots \quad 3.1$$

where the first term $f_0\,(Z, A)$ represents the mass of the constituent of the atom

$$f_0\,(Z, A) = (m_p Z + m_n\,(A - Z))\,c^2 \ldots\ldots\ldots\ldots\ldots\ldots\ldots\ldots\ldots\ldots\ldots\ldots\ldots\ldots\ldots 3.2$$

where m_pZ is the mass of the protons and m_n $(A - Z)$ is the mass of the neutrons in the core. Subsequent terms in the semi empirical equation tend to correct the mass of the nucleus due to the various effect of a liquid drop. The binding energy per nucleon in this context is assumed to be constant. Therefore, the binding energy of the whole core increases by the volume term

$$f_1\,(Z, A) = -c_1A \quad \ldots\ldots 3.3$$

where $c_1 = 15.5$ MeV/ c^2

The nucleons closer to the nucleus surface have fewer neighbors. Therefore, their binding energy is reduced by the surface term

$$f_2\,(Z, A) = +c_2A^{\frac{2}{3}} \quad \ldots\ldots 3.4$$

where $c_2 = 16.8$ MeV/c^2

The repulsive Coulomb interaction between the positively charged protons reduces the total binding energy of the nucleus

$$f_3(Z, A) = +c_3\frac{Z^2}{A^{\frac{1}{3}}} \quad \ldots\ldots 3.5$$

where $c_3 = 0.715$ MeVc^2

Nuclei do not always have the same amount of protons and neutrons; therefore an interaction arising from this asymmetry term reduces again the total binding energy of the nucleus

$$f_4(Z, A) = +c_4\frac{(Z-\frac{A}{2})^2}{A} \quad \ldots\ldots 3.6$$

where $c_4 = 23$ MeV/C^2. This term is zero for $Z = N = (A - Z)$.

The fifth term incorporates the tendency of nuclei to have even/odd Z and even/odd N

$$f_5\,(Z, A) = \begin{cases} -c_5A^{\frac{1}{2}} & even\ Z\ and\ N \\ 0 & \begin{cases} even\ Z, odd\ N \\ odd\ Z, even\ N \end{cases} \\ +\,c_5A^{\frac{1}{2}} & odd\ Z\ and\ N \end{cases}$$

where, c_5 = 11.3 MeV/c^2

3.2. Nuclear structure

The complex arrangement and interactions between bound nucleons set discrete energy levels for a nucleus. The energy level of the whole nucleus depends on the energy state of each nucleon. Nucleons in a nucleus, fill the energy levels according to Pauli's exclusion principle described in the shell model. A set of three quantum numbers is given to every particle, including nucleons. The quantum numbers (*n, l,* and *m*) define the quantum state of the particle. According to Pauli's exclusion principle, in a multi-particle system there can never be more than one particle in the same quantum state. There can be two protons (neutrons) with the same quantum numbers *n, l.* However, these particles must have a different spin quantum number *m*.

Nucleus stability primarily relies on the binding energy between nucleons. The binding energy is the sum of the attractive nuclear strong interaction and the repulsive coulomb interaction. The nuclear strong interaction has a very short range, therefore, bigger and heavier cores are less stable. This implies that the stability of any particular nucleus will decrease with an increasing neutrons in the core.

Unstable nuclei will therefore decay to more stable nuclei by different modes. These decays are normally preceded with the emission of highly energetic particles thereby allowing the remaining nucleons to bind more tightly. The emission of particles may also leave the nucleons of the newly formed isotopes in excited states. These nucleons eventually cascade to their ground state by emitting highly energetic electromagnetic γ ray radiation. Therefore, an element is radioactive when the nuclei are either unstable or in an excited state. The process of emission of particles or electromagnetic radiation to de-excite or stabilize the core is termed as radioactivity or radioactive decay.

3.3. Alpha decay

Alpha decay occurs when an unstable nucleus (parent nucleus) decays into its daughter nucleus by the emission of α particle. The alpha particle is composed of two protons and two neutrons. α particle emission is spontaneous and the nucleus ${}^{A}_{Z}X$ is transformed into ${}^{A-4}_{Z-2}X$. Therefore, α decay is characteristic of heavy nucleus disintegrating into two parts, due to the strong repulsive Coulomb interaction between protons.

Following decay by alpha emission, the mass of the parent nucleus is greater than the sum of the mass of both the daughter nucleus and the α particle. The remaining mass is transformed into kinetic energy is carried away by the lighter α particle. Therefore, decay obeys the momentum conservation law.

3.4. Beta decay

The β decay occurs when a parent nucleus decays into a daughter nucleus by the emission or absorption of a β particle (either an electron ($e-$) or a positron ($e+$). There are three possible β decay schemes; the emission of an electron ($\beta-$) by the nucleus ${}^{A}_{Z}X \rightarrow {}^{A}_{Z+1}X$, the capture of an electron (β^+) by the nucleus, ${}^{A}_{Z}X \rightarrow {}^{A}_{Z-1}X$, and the emission of a positron (β^+) by the nucleus, ${}^{A}_{Z}X \rightarrow {}^{A}_{Z-1}X$

Light unstable nuclei follow the β decay mode because of the decreasing strong nuclear interaction. Similar to the α decay mode, the mass of the parent nucleus is greater than the sum of the mass of the daughter nucleus and the electron/positron. The energy from the β decay is carried away partly by the β particle and an anti-neutrino or neutrino. The neutrino and antineutrino have very little mass (≤ 2 MeV/c^2), no electrical charge and a spin $s = \frac{1}{2}$. These ensure conservation of electric charge, angular momentum and energy.

3.5. Gamma radiation

The disintegration of the parent nucleus via α or β decay often leaves the daughter nucleus in an excited state. Through a series of cascades, the excited nucleons go to the ground state by releasing discrete amounts of energy as photons. Each transition is accompanied by a photon emission whose frequency is equal to the quotient of the energy difference divided by Planck's constant ($h = 6.626 \times 10^{-34}$ J · sec):

This type of de excitation is commonly referred to as γ decay. The possible decay routes of ^{38}Cl for example are schematically represented in Figure 3-2.

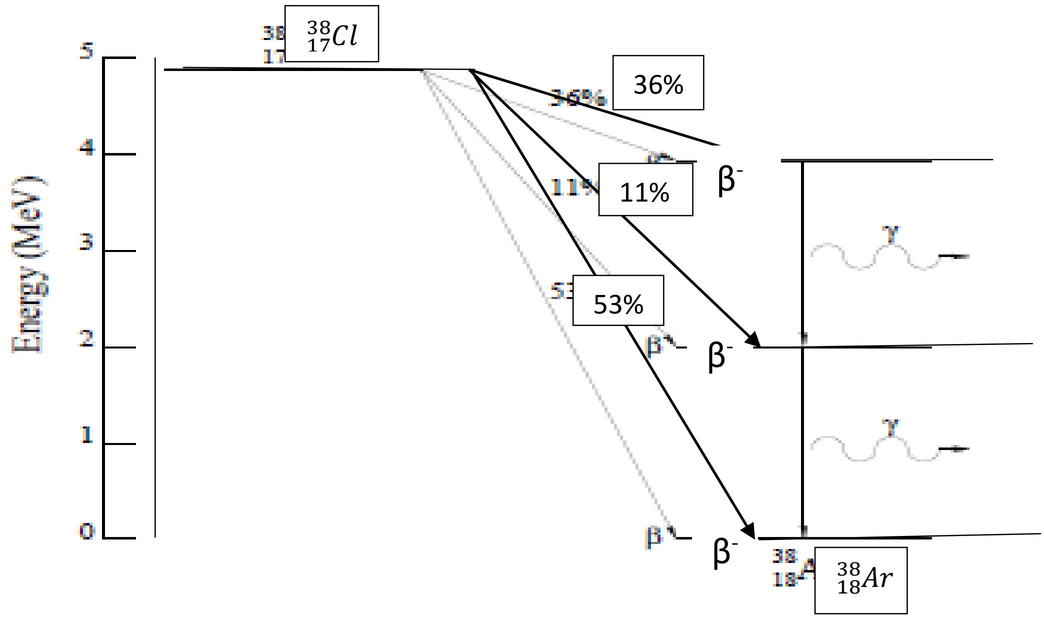

Figure 3-2: The radioactive decay of $^{38}_{17}Cl$ into $^{38}_{18}Ar$ showing the three decay possible routes and probability (David & Glen 2006).

The β decay occurs along three different possibilities; 53% chance of a 5Mev β^- particle is emitted and the parent nucleus reaches the ground state daughter nucleus. Alternatively, the parent nucleus $\beta-$ decays into an excited state of the daughter nucleus. The decay is followed by emission of γ radiation as the nucleus cascades to the ground state. However, not all transitions are allowed unless the selection rules of quantum numbers are satisfied (Δl = ±1 and Δj = 0,±1).

3.6. Radioactive Decay Rate

A radioactive nucleus has a certain probability per unit time to decay, the decay rate which is synonymous to the activity, measured in Becquerel (Bq) and represents the number of disintegration per second. The number of excited nuclei $N(t)$ remaining in the system after time t is given by.

$$N(t) = N(0)\, e^{-\lambda t} \quad \text{…………………………………………..} \quad 3.6$$

where, $N(0)$ is the initial number of nuclei in the system. The lifetime τ, can be obtained from the decay rate. This is the average time an excited nucleus survives. The lifetime is the inverse of λ. The half-life $T_{\frac{1}{2}}$ of the system is the time it takes for half of the excited or unstable nuclei to de-excite or disintegrate.

3.7. Terrestrial Radiation

Natural radioactivity has been present in the environment since time immemorial. The radioactive isotopes disintegrate via α or β decay to form stable elements. The thorium-232 series (figure 3-4), the uranium-238 series (figure 3-3) and the uranium-235 series are the three decay series found in nature. There are normally denoted as, the $4n$, $4n$ + 2 and $4n$ + 3 respectively. a $4n$ + 1 series, with ^{237}Np as parent nucleus, was present in nature at the formation of the Earth but due to the short half-life of 2.25×10^{6} yr, this series completely decayed, and is not found any more.

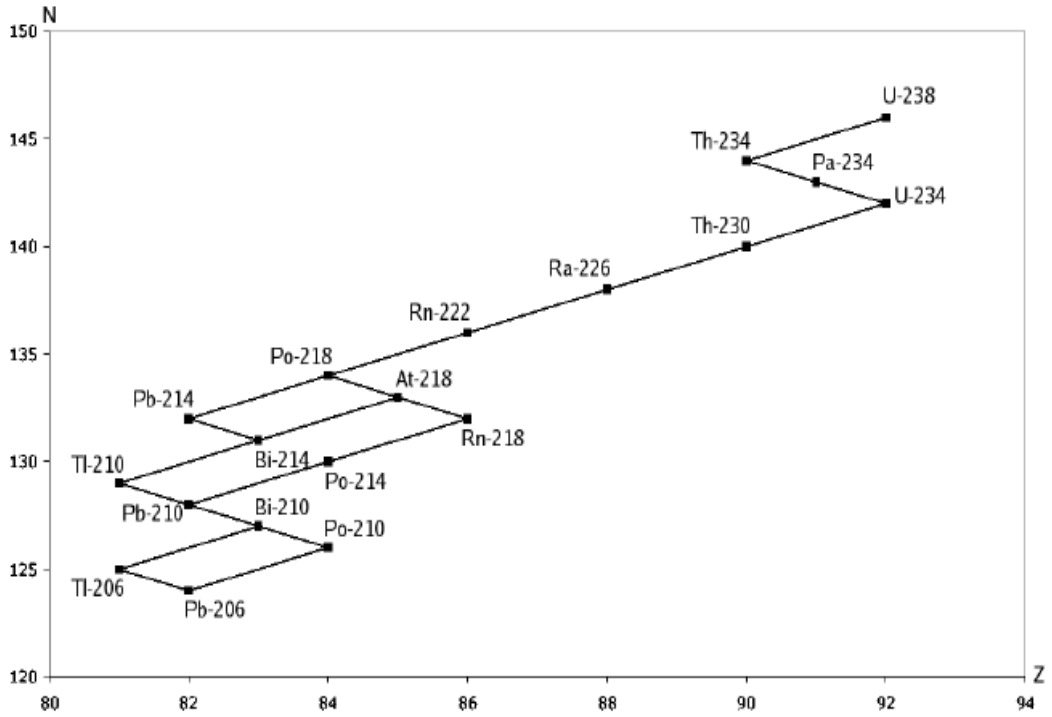

Figure 3-3: The decay series scheme of uranium-238 and its progeny's. A change to the Left represents an α decay whereas a change to the right is a β decay (David & Glen 2006).

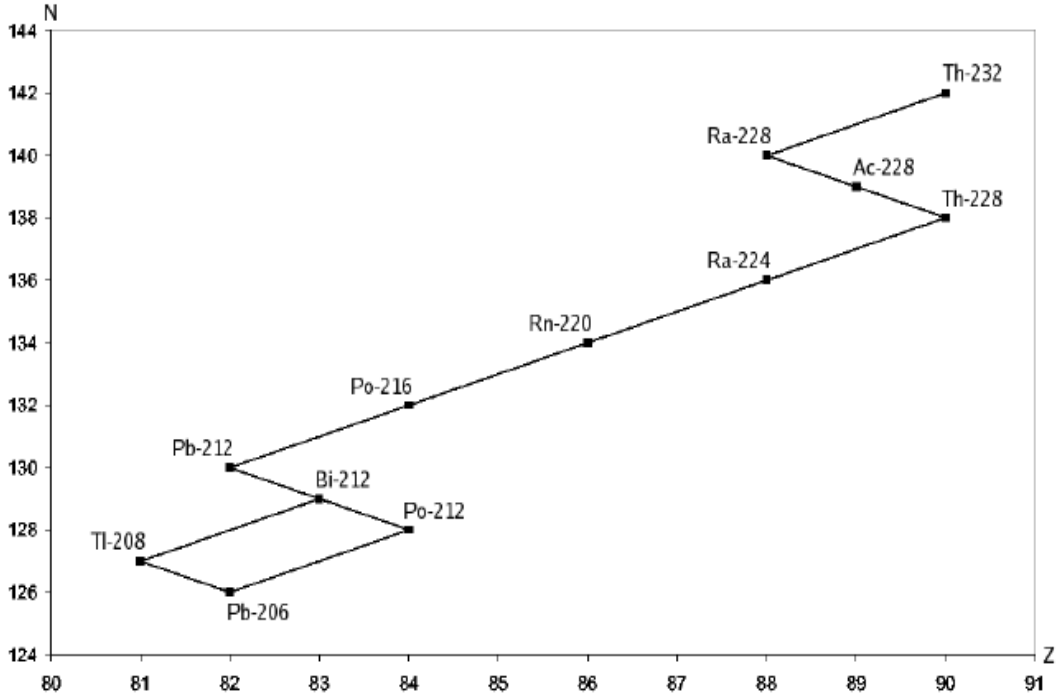

Figure 3-4: A scheme of the decay series of thorium-232 (^{232}Th) and its daughter nuclei (David & Glen 2006).

3.8. Gamma rays and their interaction with matter

As previously discussed, decays via α or β^- decay, frequently results in an excited state daughter nucleus. Through sequential γ ray emissions the daughter nucleus attains the ground state. The emitted γ ray energies have precious information on the excited state of the nucleus. For purposes of evaluating the total exposure to a population, the type and the amount of radioactive elements present in the environment must be determined; by counting the number and fluence of incoming γ rays seen by a detector by understanding the interaction of gamma rays with matter.

A γ ray is a photon that travels through free space in a straight line has energy proportional to its frequency ν and inversely proportional its wavelength (λ). In comparisson to α and β radiations, γ radiation's has a greater penetrating power; α radiation is absorbed in few layers of air whereas β are absorbed in a few layers of dense matter. The penetrating power of γ radiation, favors the detection using smaller instruments. Moreover, γ ray energies are indicators of the nuclei present, and can be used to assess whether α or β decay preceeded the γ emission. These properties of γ radiation allows field measurement to survey a greater area.

The interaction of γ rays with matter follow three processes; Photoelectric effect, Compton effect and pair production.

3.8.1. Photoelectric Effect

The photoelectric effect involves the ejection of electrons an atom, after absorbing a photon of sufficient energy. The photons energy is completely transferred to the electron. The electrons are either ejected from the surface of the material, or alternatively interact with neighbouring electrons. Ejection of an electrons leads to the formation of an ionized atom in an excited state. The excited atom regains its ground state by the cascade of outer-shell electron and the emission of *X*-ray photons or by the emission of an auger electron.

The minimum energy required to eject an electron from an atom is called the work function ($W = h\nu_0$, h is Planck's constant = 6.6262×10^{-34} J · s). The work function depends on the nature of the atom. The excess energy of the incident photon, if any, is carried away by the photoelectron as kinetic energy and is given by

$$K_e = h\nu - W \qquad 0\text{-}7$$

Where h, is planks constant, v is the frequency of the photon and W is the work function.

3.8.2. Compton Effect

The Compton effect involves interactions of the incident photon and an orbiting valence electron of the atom. Part of the photon's energy is transferred to the electron, which is subsequently ejected from the atom. The scattered photon carries the remaining energy. The new photon can interact with different valence electrons of neighbouring atoms. With each interaction, an electron is ejected and another photon of lesser energy than the previous is formed. These particle collisions follow the law of momentum conservation. The electron ejected following this collision has a kinetic energy that is equals to the difference between the energy of the incidence photon and the recoil photon, minus the work function required to eject the electron from the atom.

3.8.3. Pair production

In pair production, the incident photon creates an electron and positron pair. The photon looses its energy and results in the creation of an electron-positron pair.

The positron has the same properties as the electron, with the exception of electrical charge. However, their rest mass energy is the same. These particles are produced in the vicinity of the nucleus, therefore, the positron will have a slightly higher kinetic energy.

Pair annihilation is the inverse process of pair production that occurs when a positron comes close enough to an electron. the particles annihilate, and their rest masses are turned into energy. Each photon carries away the energy liberated from the annihilation : equivalent to 0.511 MeV

3.9. Gamma radiation spectrometry

In γ spectrometry, the energy of the incident photon (γ radiation) enables for the identification of radionuclide following photoelectric effect absorption of all the energy of the incident γ radiation. Photoelectric effect is dependent on the density of the material so does the probability of photoelectric effect. Therefore, γ spectrometers are made from semiconductive material of high Z and density.

Gas-filled Detectors, Semi-conductor detectors, Scintillation detectors are the most commonly used detectors in gamma spectroscopy. The detectors are chosen with regard to the gamma energy range that is under scrutiny, resolution and efficiency requirements. The count rate performance, the suitability of the detector for timing experiments, and price are also influential.

The efficiency of a detector is a measure of how many pulses occur for a given number of gamma rays. It is described in four terms; absolute efficiency, Full-Energy Peak (or Photopeak) Efficiency, intrinsic efficiency and relative efficiency. An efficient detector must absorb a large fraction of the gamma ray energy. The detector size or suitable high Z detector material make it possible to accomplish this fete. Figure 3-5 is a full-energy peak efficiency curve for a germanium detector.

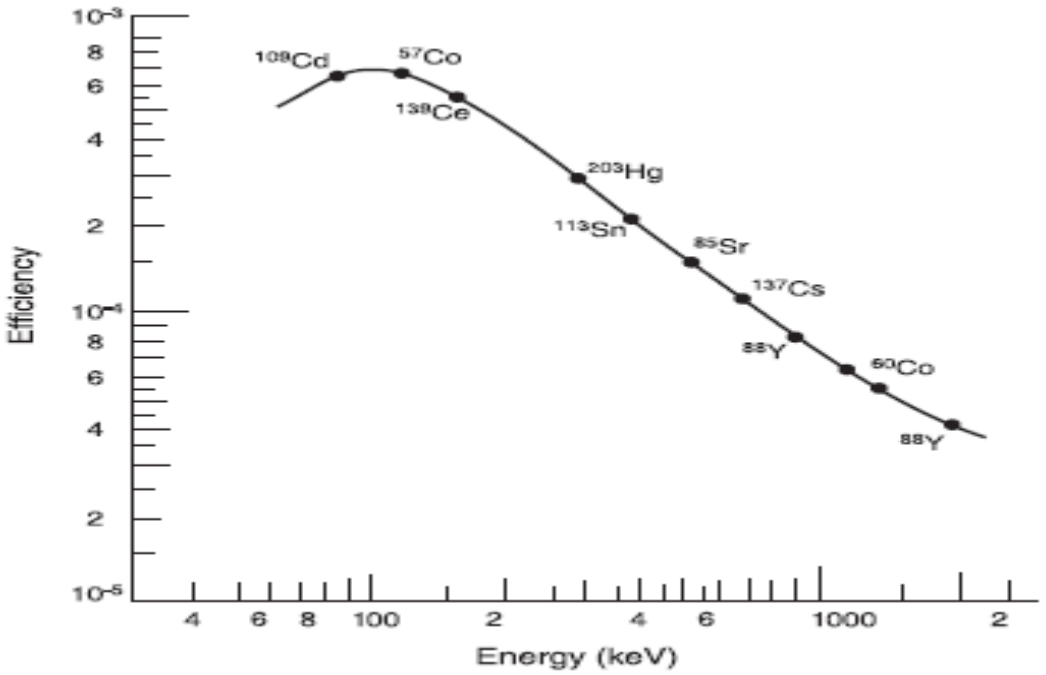

Figure 3-5: Energy calibration curve for a detector (David & Glen 2006).

The detector resolution is a measure of the width (full width half maximum) of a single energy peak at a specific energy, either expressed in absolute keV (as with Germanium Detectors), or as a percentage of the energy at that point (Sodium Iodide Detectors). If a system has a lower full width at half maximum, indicative of a better resolution, then the system will more clearly separate the peaks within a spectrum. Studies have shown a clear separation of energy peaks when using germanium detectors as compared to sodium iodide detector that show a slight overlap. In addition, when dealing with complex spectra, with peaks numbering in the hundreds, the use of a germanium detector becomes mandatory for analysis (Harb, Salahel & Abbady 2009).

The gas-filled detector is a metal chamber with a positively biased anode wire and filled with gas. Free electrons and positive ions are produced as a photon passes through the gas. The positive anode attracts electrons thereby producing an electric pulse. Recombination of electrons and the ions may occur at low anode voltages or when the density of ions is high. At sufficiently high voltages, nearly all electrons are collected. The detector then becomes an ionization chamber. The electrons are accelerated towards the anode at high energies sufficient to ionize other atoms, this causes a cascade effect characteristic of a proportional counter.

Electron multiplication becomes even greater at higher voltages. At higher voltages, electrons collection at the anode is independent of the initial ionization. The detector then becomes a Geiger-Mueller counter. All photons produce the same output pulse. At still higher voltages continuous discharge occurs. Figure 3-6 shows the operating conditions various types of detectors based on the operating anode voltage.

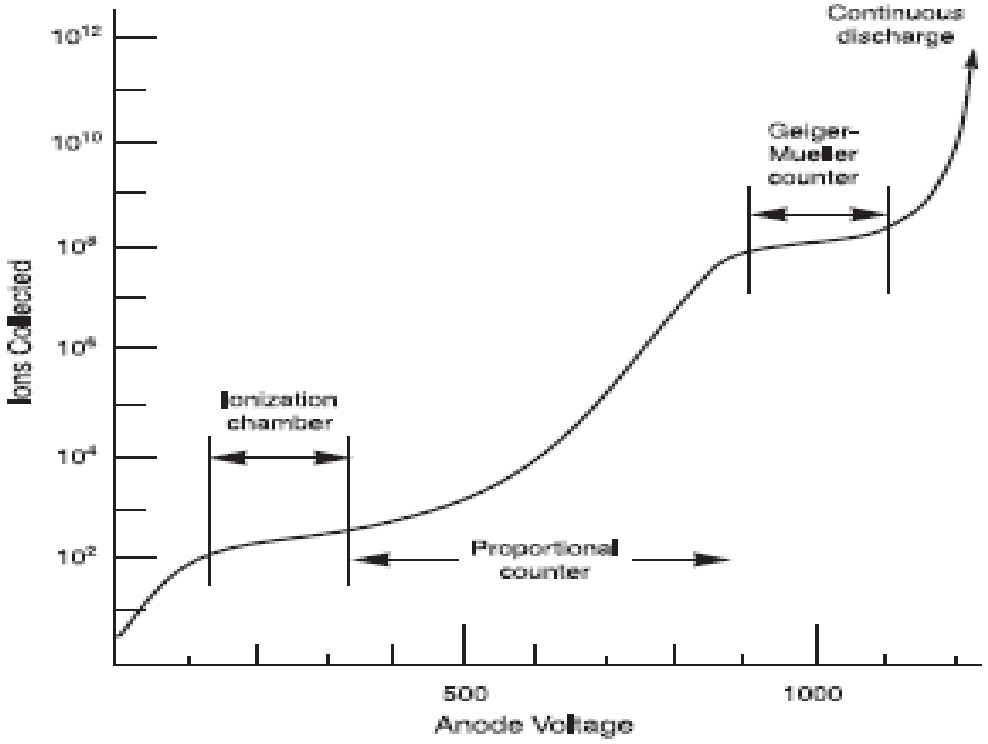

Figure 3-6: the operating anode voltages of various types of detectors (David & Glen 2006).

The very low signal output characteristic of ionization chambers, make them unsuitable for detecting individual gamma rays. However, they can be used for detecting high radiation fluxes with large current. The discharge produced by an ionization must be quenched in order for the detector to be returned to a neutral ionization state for the next pulse. This is accomplished by using a fill gas that contains a small amount of halogen in addition to a noble gas. Proportional counters are more suitable for X-ray measurements that require moderate energy resolution. The large voltage pulse common to Geiger Muller Counters make further amplification uneccessary. However, the Geiger-Mueller counter becomes inactive or "dead" following each pulse until the quenching is complete. This dead time can be hundreds of microseconds long, which limits the counter to low count rate applications.

Scintillation detectors operate through the production of light pulses when a gamma ray interacts with the scintillator. The light pulses are then converted to an electric pulse by a photomultiplier tube. The scintillation material for a good detector should be transparent, available in large sizes, and large light output proportional to gamma ray energy. Thallium activated NaI, CsI crystals, plastics. LaBr3 (Ce) crystals are currently used. NaI is still the dominant material for gamma detection because of the good gamma ray resolution and is economical. However, plastics have much faster pulse light decay and find use in timing applications, even though they often offer poor energy resolution.

Semiconductor detectors have improved energy resolution that can be attributed to the small amount of energy required to produce a charge carrier and the consequent large "output signal" compared to other detector types for the same incident photon energy. Ge semiconductors are able to distinguish between two γ rays close in energy (high energy-resolution). This is as a result of the small band gap between the valence band and the conduction band. In addition, Ge detectors have high full-energy efficiency. This is achieved by using large Ge crystals. The detector collects charges produced by the ionization of the semiconductor material. One electron-hole pair is produced on the average for every 3 eV absorbed from the radiation. These pairs drift under an external electric field to the electrodes where they generate the pulse (Khandaker 2011: Xhixha et al. 2013)**.** The HPGe detectors have high atomic number, low impurity concentration (large depletion depth), low ionizing energy required to produce an electron-hole pair, high conductivity, compact size, fast time response, high resolution and relative simplicity of operation.

CHAPTER 4

RESEARCH METHODOLOGY

4.1. Introduction

This chapter describes the methods used to assess terrestrial gamma radiation exposure levels in the coal deposit area of the Mui basin, Kitui County. Gamma spectroscopy is the method of choice used methods for TGR measurements of the samples.

4.2. Description of the Study Area

The Mui Coal Basin is located approximately 180 km northeast of Nairobi, covers 500Km^2 in area and is estimated to hold 400,000,000 metric tons of exploitable coal reserves. The Ministry of Energy (MOE) Kenya partitioned it into Blocks A, B, C and D. Detailed coal quality analyses, resource evaluation, exploration drilling, surface geological mapping and geophysical surveys have been completed. Fifty-four wells between 75m to 445m deep are in Block C and four wells in Blocks A, B and D were drilled to determine the expanse of the coal seams. Six coal seams, between 0.3m and 13m thick have been identified and coal found at depths of between 20m and 320m in 40 of the wells. Block C is bordered by Lundi and Yoonye at the northern and southern extremities, respectively (Muthangya & Samoei 2006).

The Mui basin lies along the Mozambique belt of Kenya and is encircled by Precambrian crystalline (Neoproterozoic Mozambique Belt rocks) Mui lacustrine sediments rocks consisting of biotite gneisses, migmatites, meta-granite, granitoid gneisses, quartzites, pegmatites, sillimanite gneisses and schists (Figure 4-1). The belt consists of sedimentary rocks that have metamorphosed over time. Granitoid gneisses, resistant to erosion constitute the surrounding hills. A major fault runs N-S through Mutito and Ikoo and adversely influences the drainage system (Ndolo *et al*., 1997).

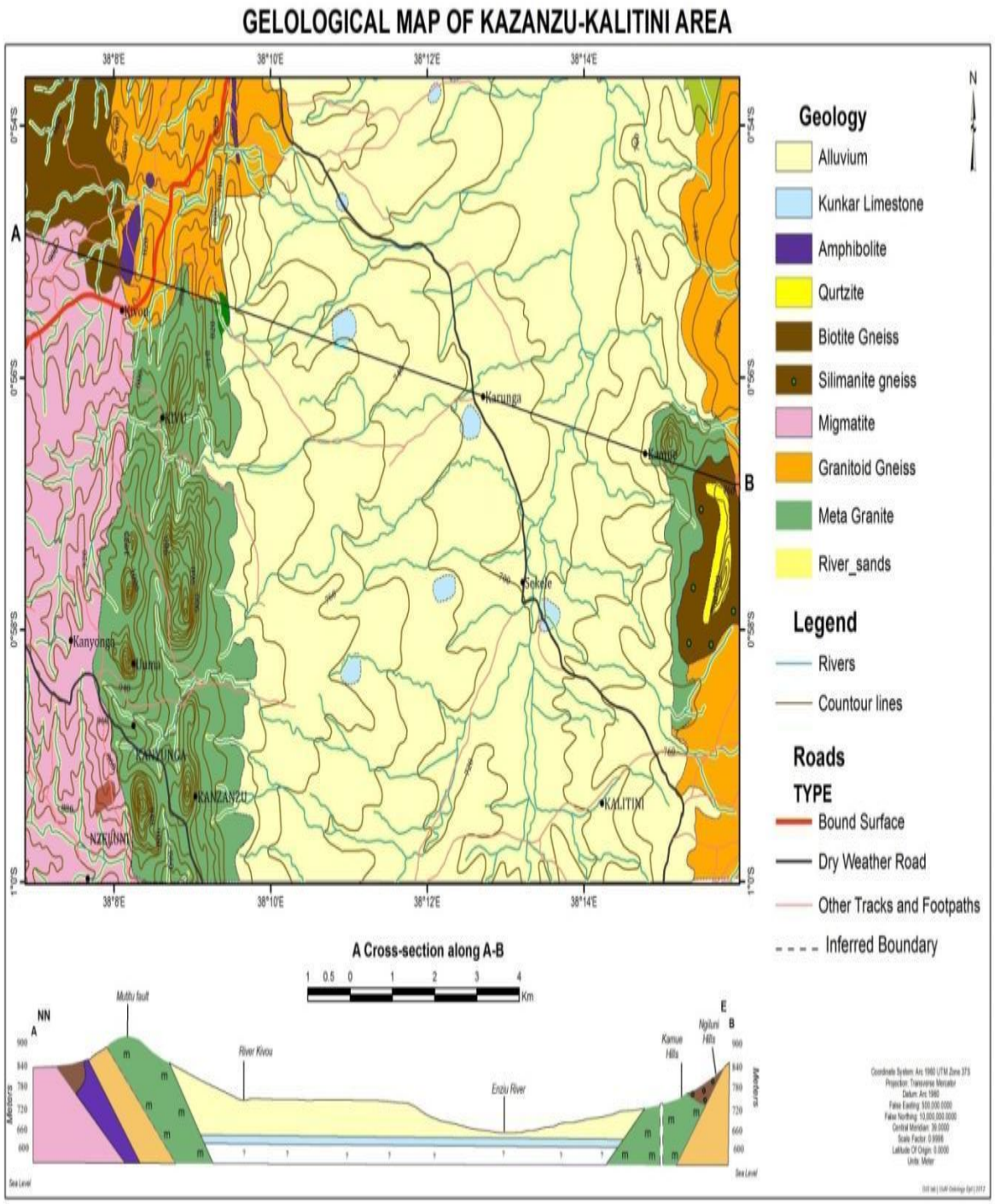

Figure 4-1: The geological characteristics of Kazanzu- Kalitini area (Ndolo *et al.*, 1997).

The soils of the Mui basin can be categorized into sands, clays, silt and a mixture loam. The nature of the underlying rocks contributes to the unique composition of the soil cover. The alluvial sandy soils include river deposits and outwash from the hills. Sandy soils dominate the western and north-western parts of the Mui basin that results from outwash in the nearby Mutito Hills. Clay soils are also found to border the sandy regions and clay sand and loam mixtures also exist in the region (Ndolo *et al*., 1997).

The natural vegetation comprises of dry bush and thickets mainly acacias and trees shrubs common to most of semi-arid areas in Kenya. Based on the climatic conditions the indigenous vegetation is drought resistant whose distribution is primarily influenced by rainfall, geology, soils, and topography (Ndolo *et al*., 1997).

4.3.Sampling

Forty-two soil samples were collected randomly in Block C of the Mui basin Kitui between August 19th and 22nd 2013 specifically from Yoonye, Kateiko and Kathonzweni areas of in an area covering approximately the 131.5km^2. The soil samples each weighing approximately 500g were collected at a depth of 10cm to 20cm were packed into non-radioactive plastic sample bags appropriately labeled for later identification. Appendix A-1 shows the sampling coordinates of areas sampled in this study. Figure 4-2 shows the sampling points. A Garmin GPRS meter was used for mapping sampling points in Block C of the coal deposit area. Further processing of GPRS data done using Global mapper software (V 15).

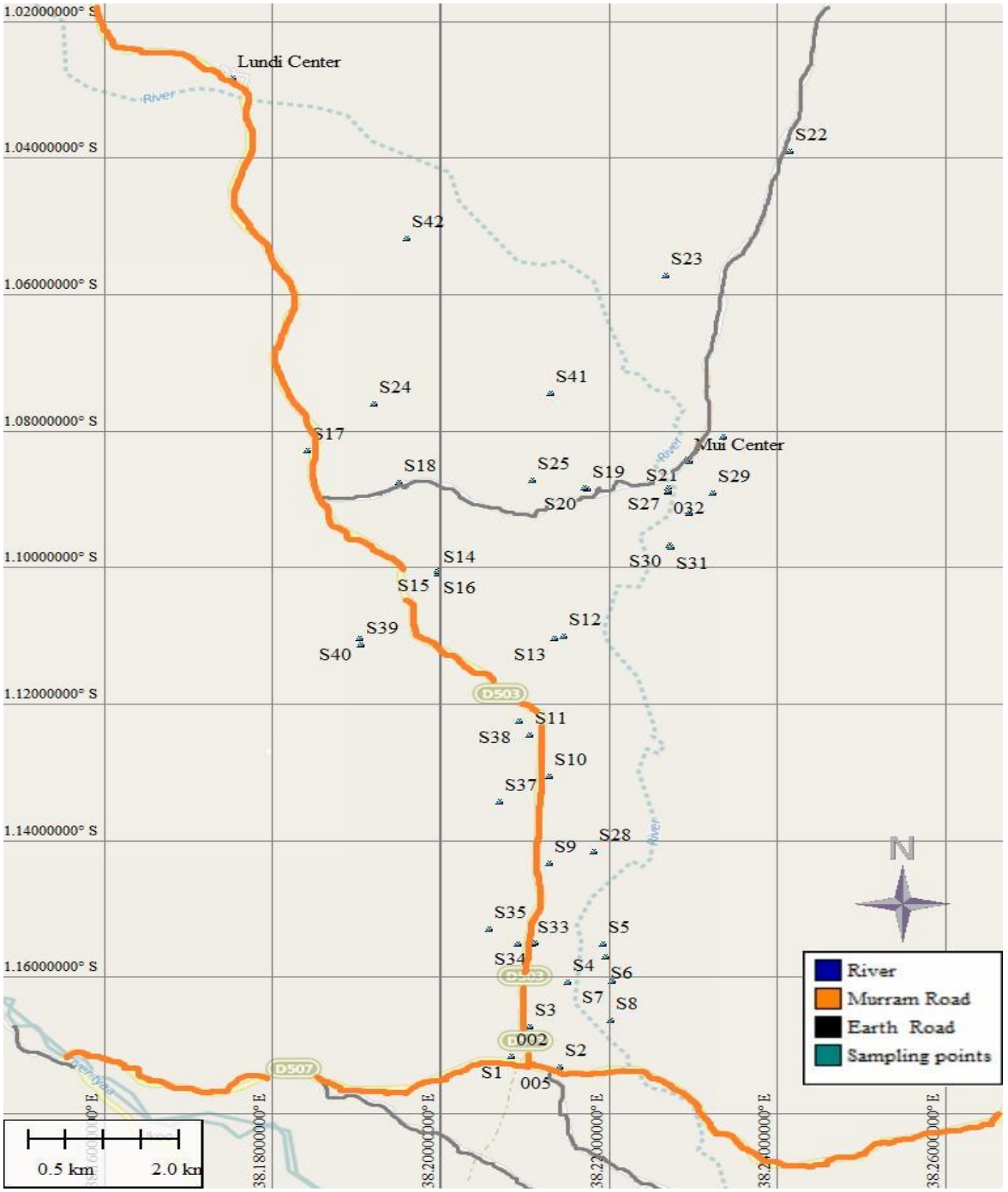

Figure 4-2 Sampling sites in the coal rich Block C of the Mui Basin

The Mui Basin is rough terrain with marram roads and most of the sections have thorny acacia trees that are almost impassable. The seasonal rivers concealed under sand, makes crossing them difficult. access to certain areas of the basin are restricted.

4.4. Sample Treatment

The samples were dried in an oven at 60^0C to constant weight to remove moisture. They were further crushed and pulverized to homogeneity and sieved through a 0.5 mm sieve.

About 300g of soil samples were measured and stored in a standard 500g plastic container that was tightly sealed for 30 days for the radionuclides and their short-lived progeny to reach secular equilibrium before counting was done. Aluminum foil was also used to seal the lid of the holding container to ensure ^{222}Rn did not escape. The dimension of the containers used were similar to those used for the containers of the IAEA reference samples; RGU-1, RGK-1 and RGTh-1 for calibration purposes and measurements.

4.5. Gamma ray spectroscopy

The gamma spectroscopy unit used comprises of a HpGe detector encased within a 10 cm thick lead shielding and cooled by liquid nitrogen. The detector was connected to a preamplifier, an amplifier and power supply and interfaced to the desktop PC for spectral data analysis with ORTEC MAESTRO software. The Unit used for this study is available at the Institute of Nuclear Science and Technology, University of Nairobi and is shown in Figure 4-2.

Figure 4-3 Gamma-ray spectroscopy unit at the Institute of Nuclear Science and Technology, University of Nairobi

4.5.2. Specifications of the HPGe detector

The radioactivity in the soil samples was measured using a gamma-ray spectrometer HPGe detector Model No. CPVD530-30185 SN 2489 with the following characteristics;

a) Crystal characteristics: The detector is a coaxial (5 .74 X 5.79 cm) HPGe with 30% efficiency relative to the 3" x 3" NaI (Tl) detector with an active volume of 144 cm^3. The germanium dead layer is 600microns in thickness with the detector to window distance of 5mm. Its original measured resolution was 1.8 KeV (FWHM) at 1.33 MeV peak of Co-60. The MCA is a PC based card supplied to operate with MAESTRO software personal computer analyzer (PCA3) for data acquisition and analysis. Further data analyses were also performed with the MS Excel.
b) End Cap Characteristics: The outside diameter of the endcap was 76mm with a front window of 1mm thick Al.

The detector required a six hour cool down before the application of bias high voltage. In terms of performance, the operating high voltage bias was at 3200 with a positive polarity. The spectroscopic amplifier is a Tennelec TC-244 set to 6µsec Gaussian shaping form. The power supply unit is Tennelec TC 950. The pulse height analyzer was a Nucleus PCA-8000 with 8192 channels.

The detector energy calibration was done using the 1332 KeV and 1172 KeV energy lines of ^{60}Co in a standard sample container prior to measurements. The samples were run for between 36000 and 43500 seconds, time considered sufficient for counting sample radionuclide activity concentration.

The MAESTRO software was used to determine spectral radionuclides intensities. Using the intensities of the radionuclides of interest in the standard reference materials, the activity concentrations of radionuclides in unknown samples were calculated by comparison.

4.6. Assessment of Radiation health hazard risks due to terrestrial gamma radiation exposure

Certain parameters are universally used to assess the radiation health hazard risks associated with exposure to terrestrial gamma exposure. These parameters are derived from models developed from extensive epidemiological and mechanistic studies of

populations previously exposed to large doses of radiation. In this section, we describe the method used in evaluating health risk associated to exposures to terrestrial gamma radiation.

4.6.1. Specific Activity concentration

The activity concentrations of the radionuclides in the soil samples were determined through direct comparison method with the IAEA reference standards, namely RGK-1, RGU-1 and RGTh-1 of known ^{40}K, ^{238}U and ^{232}Th activities in the soil samples respectively. Since the counting rate is proportional to the amount of the radioactivity in the samples. Activity Concentration (Ac) was determined from the following equation:

$$A_S = \frac{A_R M_R I_S}{M_S I_R} \qquad \text{.....4. 1}$$

Where A_S, I_S, and M_S is the unknown activity of a radionuclide in the soil sample, the radionuclide spectral intensity and mass of soil samples used. A_R, M_R, and I_R are the activity concentrations of radionuclide, mass and radionuclide intensity of the IAEA reference soil samples. The activity concentration for each of the radionuclides of interest were determined independently. The specific activity concentration of the natural radionuclides present in the soil samples was determined using gamma ray energy transition lines associated with decays and decay products of uranium and thorium series as well as long-lived ^{40}K. The specific activity of ^{232}Th was determined based on gamma lines of energies of 911 and 238.6 KeV. For the determination of activity concentration of ^{238}U, the gamma ray lines at 351.9KeV, 609KeV were used. The transition lines at 1460.82KeV was used to determine the activity concentration of ^{40}K (Tsai et al., 2008).

4.6.2. Detection limit (LD)

When working with low-level gamma samples such as soil, the detection limit of the detector is an essential factor. The detection limit is a calculated estimate of the detection capability of the measurement system; defined by the following equation

$$DL = \frac{\sqrt{Bg}}{PA} \times 3 \times CA \quad \text{..... 4-2}$$

where, Bq is the number of counts over the count period for the background, PA is the peak area and CA is the activity concentration for each radionuclide.

4.6.3. Gamma absorbed dose rate

The gamma absorbed dose rate as per UNSCEAR (2000) report was calculated was derived using the equation below:

$$D\ (nGyhr^{-1}) = 0.042A_K + 0.604A_{Th} + 0.462A_U \quad \text{..... 4-3}$$

where D is the absorbed dose rate measured at a point 1 m from the earth surface in nGy/hr. A_K, A_{Th} and A_U are the activity concentration of ^{40}K, ^{232}Th and ^{238}U respectively. The contribution from other radionuclides, such as ^{137}Cs, ^{90}Sr and the ^{235}U series can be neglected as they contribute very little to the total dose from the environmental background. ^{238}U is replaced by ^{226}Ra since the contribution of ^{226}Ra to the external dose is about 98%.

4.6.4. Annual effective dose equivalent

The outdoor and indoor AEDE (mSv) from the radioactivity content of the soil was calculated using the following formula:

AEDE= D x DCF x OF x t

AEDE (μSv / y) = D (nGy / h) × 8760(h / y) × 0.2 × 0.7(Sv /Gy) × 10^{-3}……4.4

where, D is the absorbed dose rate (nGy/hr.), OF is the outdoor or indoor occupancy factors, assumed to be 0.2 and 0.8 respectively, DCF is the dose conversion factor (0.7 Sv) and *t* is the duration of the exposure time in hours (UNSCEAR, 2000).

4.6.5. Radium equivalent

Radium equivalent activity (Ra_{eq}) is used to assess the hazards associated with materials that contain^{226}Ra, ^{232}Th and ^{40}K in $BqKg^{-1}$. The published maximum admissible Ra_{eq} is 370 Bq/kg. Radium equivalent was calculated from the equation below.

$$Ra_{eq} = A_{Ra} + 1.43A_{Th} + 0.07A_K \quad \text{..... 4-5}$$

where A_K, A_{Th} and A_R are the specific activities of ^{40}K, ^{232}Th and ^{226}Ra ($Bqkg^{-1}$), respectively. In defining Ra_{eq} activity, it is assumed that 370 $Bqkg^{-1}$ of ^{226}Ra, or 259 $Bqkg^{-1}$ of ^{232}Th, or 4810 $Bqkg^{-1}$ of ^{40}K will all produce the same dose rate (UNSCEAR, 2008).

4.6.6. External Hazard Index (H_{ex})

The external hazard index is an evaluation of the hazard of the natural gamma radiation. Having determined the radium equivalent from the measured specific activity, the external and internal indices were calculated. The main objective of these indices is to limit the radiation dose to permissible dose equivalent limit of 1 *m*Sv (ICRP 1990). In this context, a number of models have been proposed and reported in the open literature. In this study, the following relation was used (UNSCEAR 2011).

$$H_{ex} = \frac{1}{370}(A_R \pm 1.43A_{Th} \pm 0.07A_K) \leq 1 \quad \text{..... 4-6}$$

where A_K, A_{Th} and A_{Ra} are the activities of ^{40}K, ^{232}Th and ^{226}Ra in Bq/kg, respectively.

4.6.7. Internal hazard index (H_{in})

Internal hazard index (H_{in}) gives the internal exposure due to the indoor radon and its short- lived progeny, was measured using the relation (UNSCEAR, 2008).

$$H_{in} = \frac{A_{Ra}}{105} \pm \frac{A_{Th}}{259} \pm \frac{A_K}{4910} \quad \text{..... 4-7}$$

where A_K, A_{Th} and A_{Ra} are the activities of ^{40}K, ^{232}Th and ^{226}Ra in Bq/kg, respectively.

CHAPTER 5

RESULTS AND DISCUSSION

5.1. Introduction

In this chapter the results of the study are presented and discussed. The results of activity concentration obtained were used to determine the gamma absorbed dose, annual effective dose equivalent (AEDE) and gamma radiation hazard indices.

5.2. Gamma Spectrum

Figure 5-1 is a gamma spectrum obtained for sample S1 presented as a plot of the counts against energy. Using the radionuclide spectral intensities for each soil sample and of the reference standards, the activity of each radionuclide was determined.

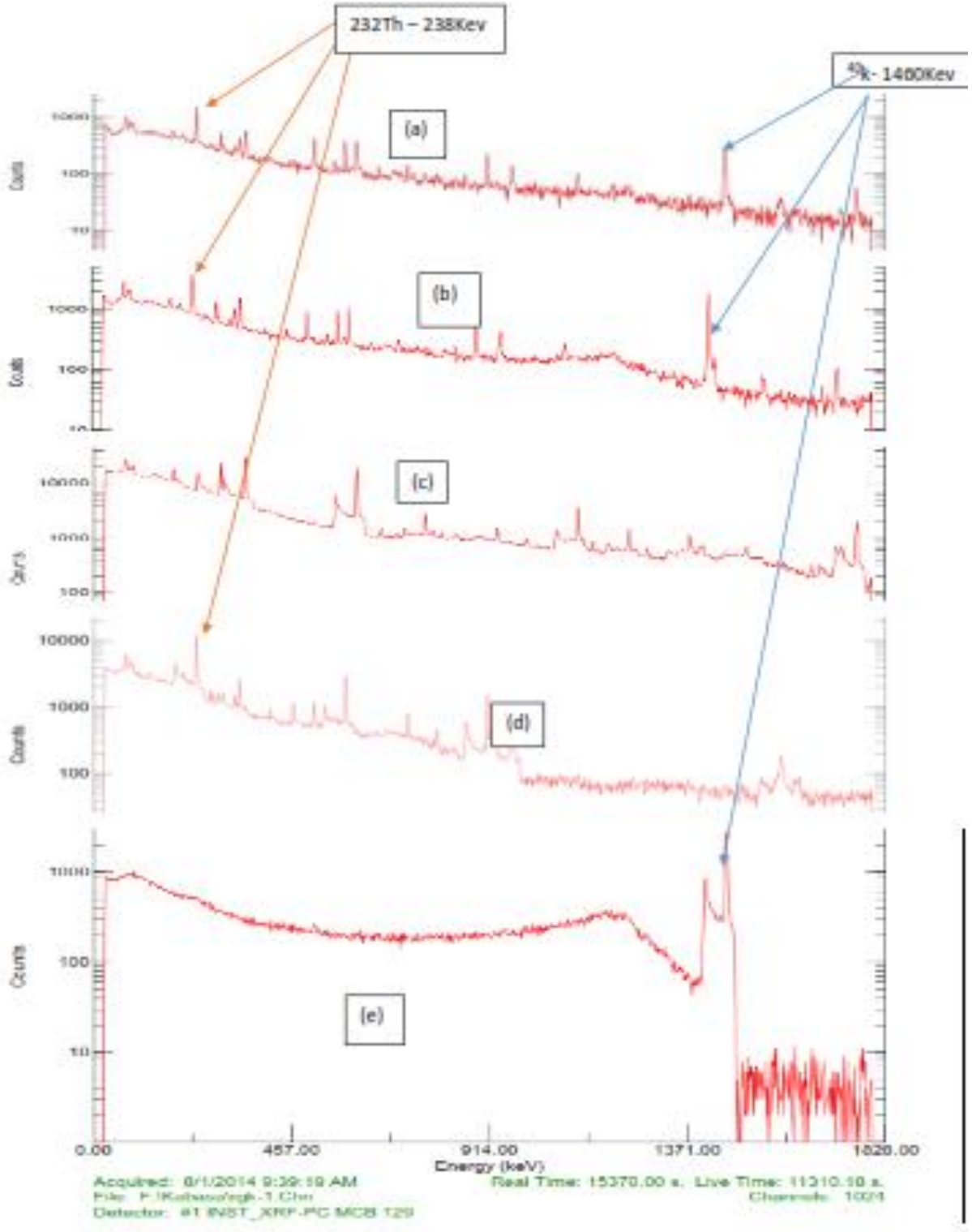

Figure 5-1: Gamma spectrum for S2 (a), S5 (b), RGU-1 (c), RGTh-1 (d) and RGK-1 (e).

5.3. Activity Concentration of Radionuclides

The detection limit of the HpGe detector was determined to be 5, 5 and 30 Bqkg^{-1} for ^{238}U, ^{232}Th and ^{40}K respectively. Table 5-1 shows the results of the average, maximum and minimum activity concentration determined for the forty-two (42) soil samples collected in Block C of the Mui Basin. ^{40}K was the most abundant in the soil samples.

Table 5-1: Summary of results of radionuclide activity concentrations in Bqkg^{-1}

Descriptive Statistics	^{232}Th	^{238}U	^{40}K
Mean (Bq/kg)	68.7	39.9	973
Standard deviation	28.5	15.2	401
sample variance	812	229	161233
Min (Bq/kg)	9.7	14.2	348
Max (Bq/kg)	130	75.9	1678
Range	120.3	61.7	1330

The results of the measured radionuclide activity concentrations for all the individual soil samples are in Appendix A-2. In general, the average activity concentration of ^{40}K and ^{232}Th was about two times higher than the world average of 35 Bqkg^{-1} and 400 Bqkg^{-1}. However, the average activity concentration of ^{238}U was within the 30 Bqkg^{-1} global averages. The high sample variance observed for ^{40}K is as a result of the wide range observed in its activity concentration in the soil samples.

Figure 5-2 shows the relative abundance of the natural radionuclides in the measured soil samples. About 90% of the total measured activity concentrations were contributed by ^{40}K; 4% by ^{238}U and 6% by ^{232}Th.

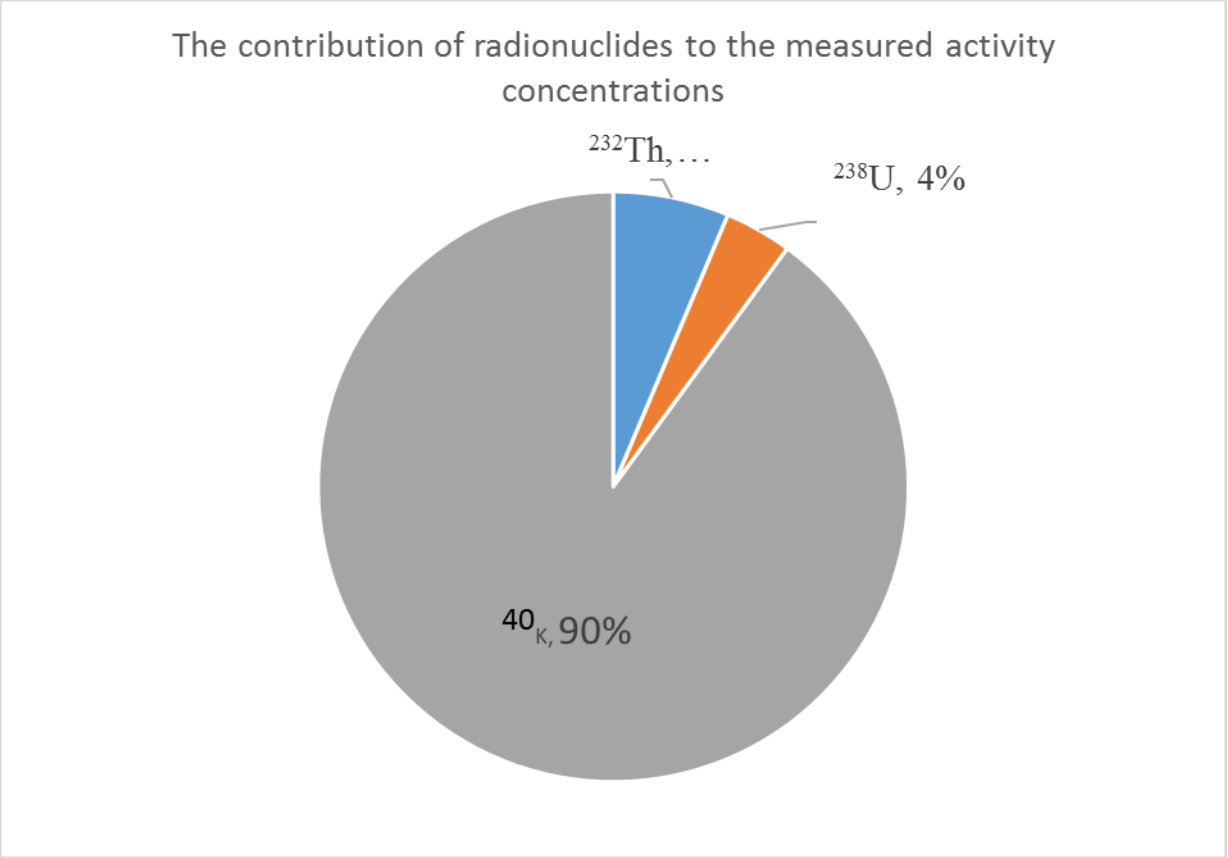

Figure 5-2: Radionuclide abundance in the soil samples from Mui Basin

The results of radionuclide measurements of the samples from the three distinct regions namely; Kateiko, Yoonye and Kathonzweni are presented in Table 5-2. In general, soil samples from Yoonye had the highest ^{40}K activity concentration approximately 1124BqKg^{-1}. There was no significant difference in activity concentration of ^{232}Th between the regions sampled. However, there was significant difference between ^{40}K concentrations ($p = 0.02$) of soil samples from Kateiko and Yoonye.

Table 5-2 Summary of Activity Concentration at Different Localities in Block C, Mui Basin

ACTIVITY CONCENTRATIONS SUMMARY (Bqkg^{-1})			
Sample Localities	**^{232}Th**	**^{238}U**	**^{40}K**
Kateiko	72.0	41.4	897
Yoonye	68.7	37.9	1124
Kathonzweni	71.1	42.1	762

Figure 5-3 and 5-4 show the variation in activity concentrations of the radionuclides of interest in soils analyzed in this study.

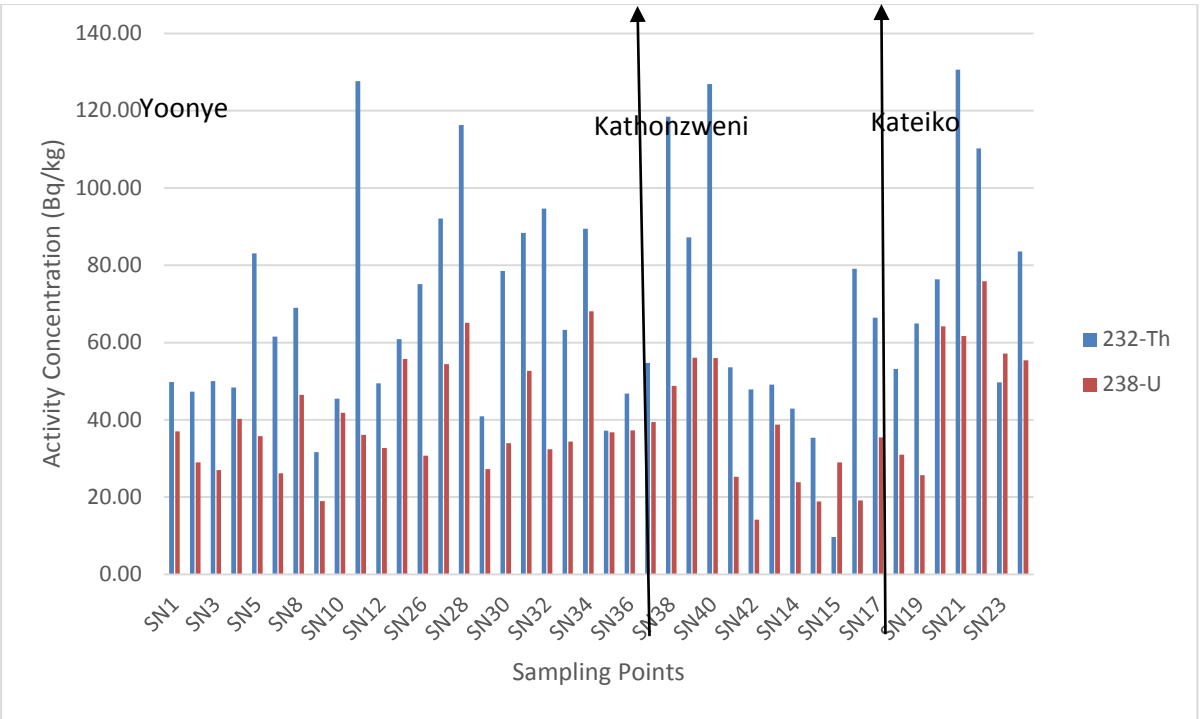

Figure 5-3: Variation in radionuclide activities in soils of Mui Block C

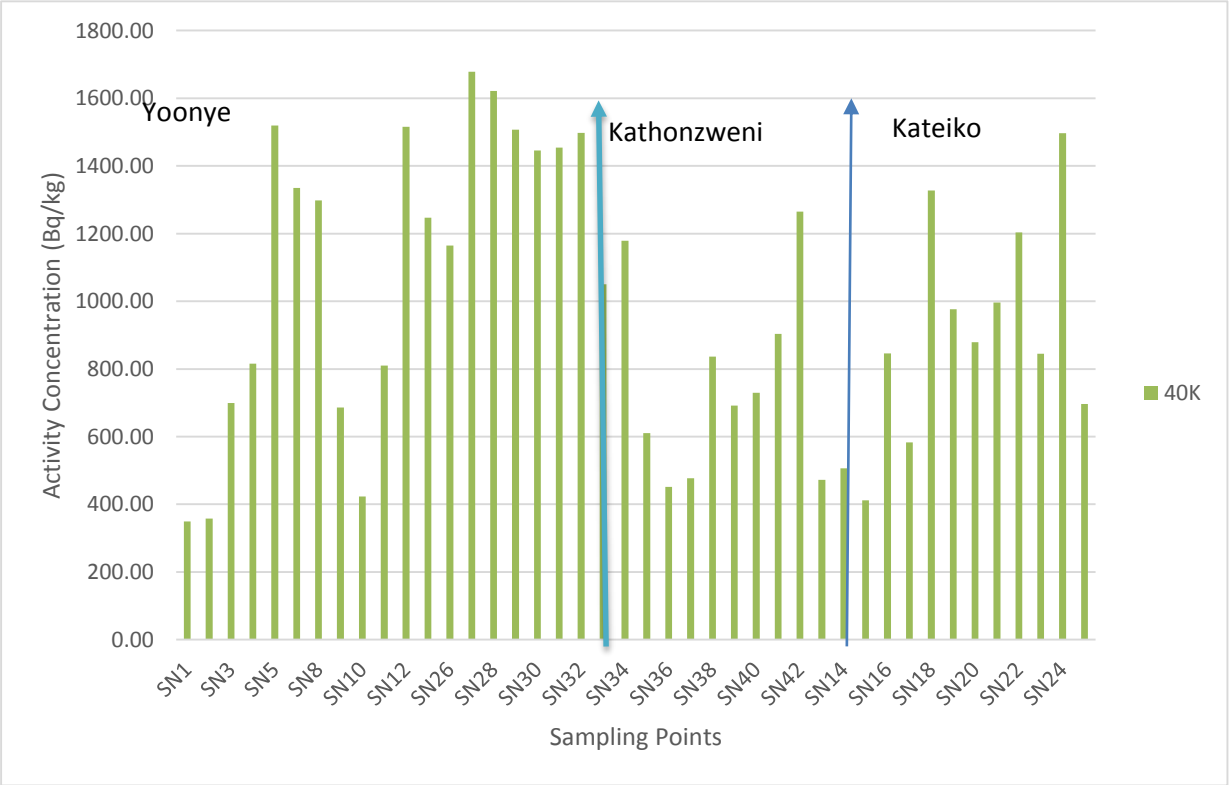

Figure 5-4 variation in activity concentration of 40K in the Mui Basin Block C

These results are consistent with most local measurements of natural radionuclide activity concentrations in soils such as those reported by Kinyua, Atambo & Ongeri

(2011) and Chege et al. (2014). In this study, approximately 74% (z= -0.65) of the ^{238}U activity measurements were above the world average of 30 $Bqkg^{-1}$, 89% (z= -1.18) of the ^{232}Th were also found to be above the world average of 35 Bq/kg. For the ^{40}K activity concentrations 92.3% (z=1.43) of the values were above the world average of 400Bq/kg. The values for z were obtained by assuming a normal distribution of the results obtained.

5.4. Absorbed Dose Rate, Annual Effective Dose Equivalent, Radium Equivalent, Hazard Indices

Table 5-3 shows the results of the mean absorbed dose rate ($nGyhr^{-1}$) as determined from the activity concentrations measurements. In general, the gamma absorbed dose rate ranged between 48 and 173 $nGyhr^{-1}$in Block C with an average of 103 $nGyhr^{-1}$ for all soil samples analyzed in the study (Appendix A-3).

The annual effective dose equivalent ($mSvyr^{-1}$) ranged between 0.06 and 0.21 $mSvyr^{-1}$ with an average of 0.13 $mSvyr^{-1}$. Radium equivalent values were found to vary between 98.3 and 344 $Bqkg^{-1}$ with an average of 228 $Bqkg^{-1}$. The external radiation hazard indices were found to range between 0.27 and 0.96 with an average value of 0.58. The internal hazard index ranged between 0.32 and 1.14 with an average of 0.68.

Table 5-3: Assessment of radiation exposure

Descriptive Statistics	Absorbed dose ($nGyhr^{-1}$)	AEDE ($mSvyr^{-1}$)	Raeq ($BqKg^{-1}$)	H_{EX}	H_{IN}
MEAN	103	0.13	228	0.58	0.68
STDEV	32.7	0.04	142	0.18	0.21
Max	173	0.21	1029	0.96	1.14
Min	48.9	0.06	98.3	0.27	0.32

^{232}Th contributes significantly to gamma absorbed dose rate followed by ^{238}U and then ^{40}K which is also consistent with other studies. From Figure 5-5 it is observed that ^{232}Th has a strong relationship to dose R^2= 0.73. The relationship between activity concentration of ^{238}U and Absorbed dose rate (R^2 = 0.44) is shown in Figure 5-5 and that between ^{40}K (R^2 = 0.59) in figure 5-6. These variations in contribution of the activity concentrations of ^{238}U, ^{232}Th and ^{40}K to the respective gamma absorbed dose can be attributed to the gamma absorbed dose rates in the soil samples analyzed.

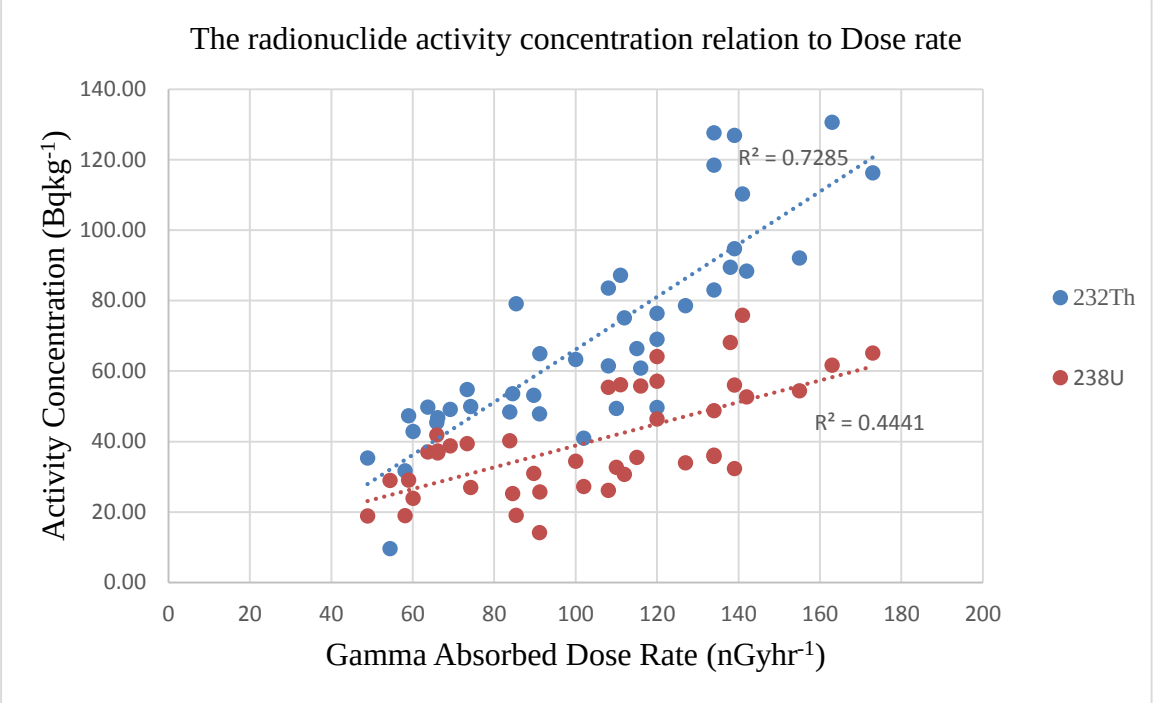

Figure 5-5: Relationship between ^{232}Th, ^{238}U activity concentrations and absorbed dose rate

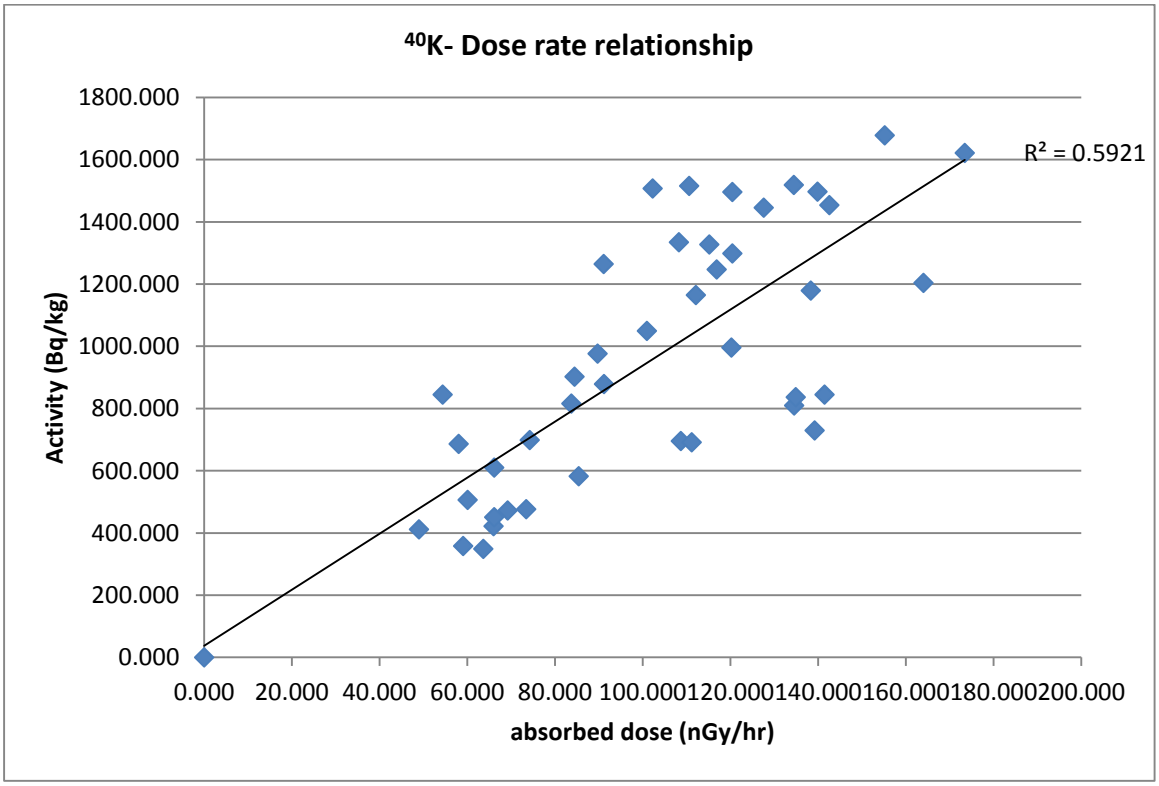

Figure 5-6: The relationship between the activity concentration of ^{40}K and absorbed dose rate

In general, the average dose rate 104 nGyhr^{-1} is higher than the world average dose rate of 60nGyhr^{-1} for which 90.7% (z= -1.33) of gamma absorbed dose rates were above the world average whereas, approximately 92.22% corresponding to a z value of -1.425 of

AEDE were found to be above the world average annual effective dose rate of 0.07mSvyr^{-1}. The mean annual effective dose equivalent was calculated to be 0.127mSvyr^{-1}. This value is higher (X2) than the world average of 0.07mSvyr^{-1}. In general, the absorbed dose and annual effective doses are above world averages. However, the average AEDE for the sample sites is lower than the 2 mSvyr^{-1} permissible limit for exposure.

The external and internal radiation hazard indices are below the recommended threshold limit with the exemption of the samples 23, 24- in Kateiko and 27, 29-Yoonye. The average Ra_{eq} (206 Bq/kg), internal hazard index (0.69)- for which 63% and the external hazard index (0.58)-for which 99% are well below the world or recommended threshold respectively (Table 5-4, Table 5-5).

The differences in the average gamma absorbed dose rates, the average AEDE, internal and external hazard indices, and radium equivalent between the three localities of Kateiko, Yoonye and Kathonzweni was found to be statistically insignificant at $p<0.05$.

.

Table 5-4: Radiation Exposure Parameters at various localities of the Study area

LOCATION	DOSE RATE (nGy/hr)	AEDE (mSv/yr)	Ra eq (<370Bq/Kg)	Hex (<=1)	Hin
Yoonye	108.84	0.134	214.70	0.601	0.704
Kathonzweni	97.24	0.1195	197.10	0.5467	0.6604
Kateiko	87.42	0.107	175.89	0.489	0.585

There is a weak correlation between inter-nuclides assessed in this study (Figure 5-7, 5-8).

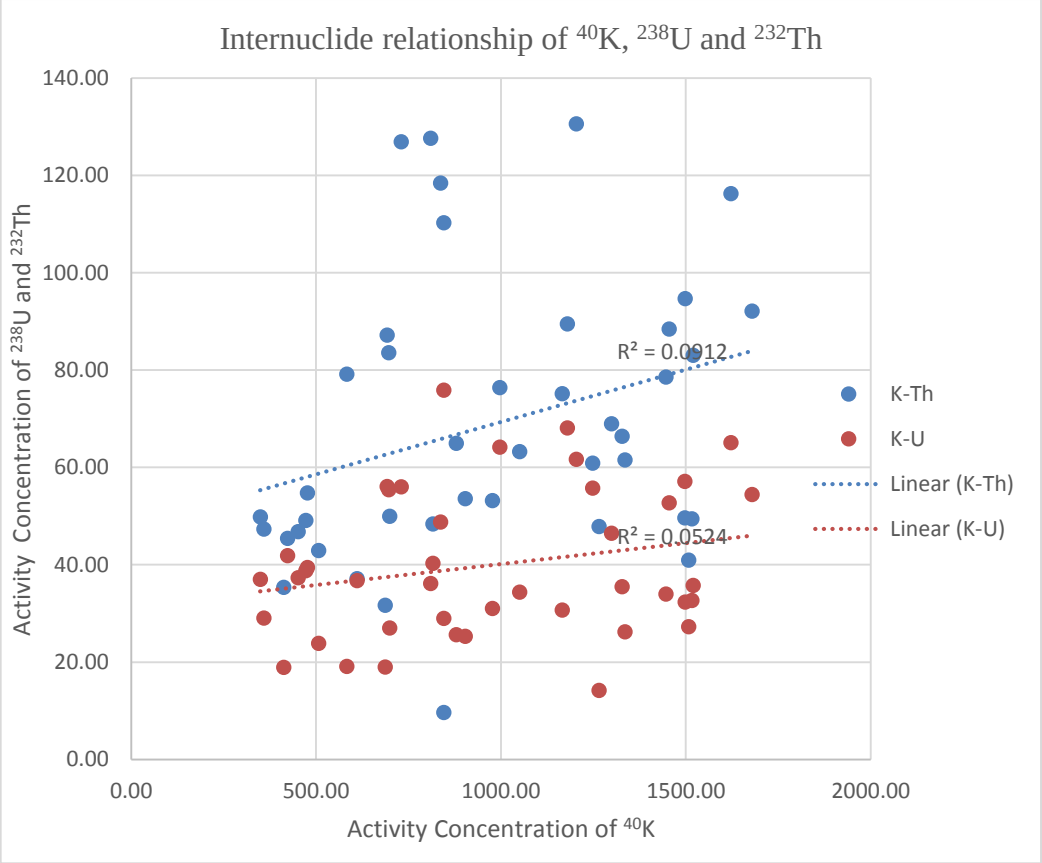

Figure 5-7: The relationship between ^{232}Th and ^{238}U

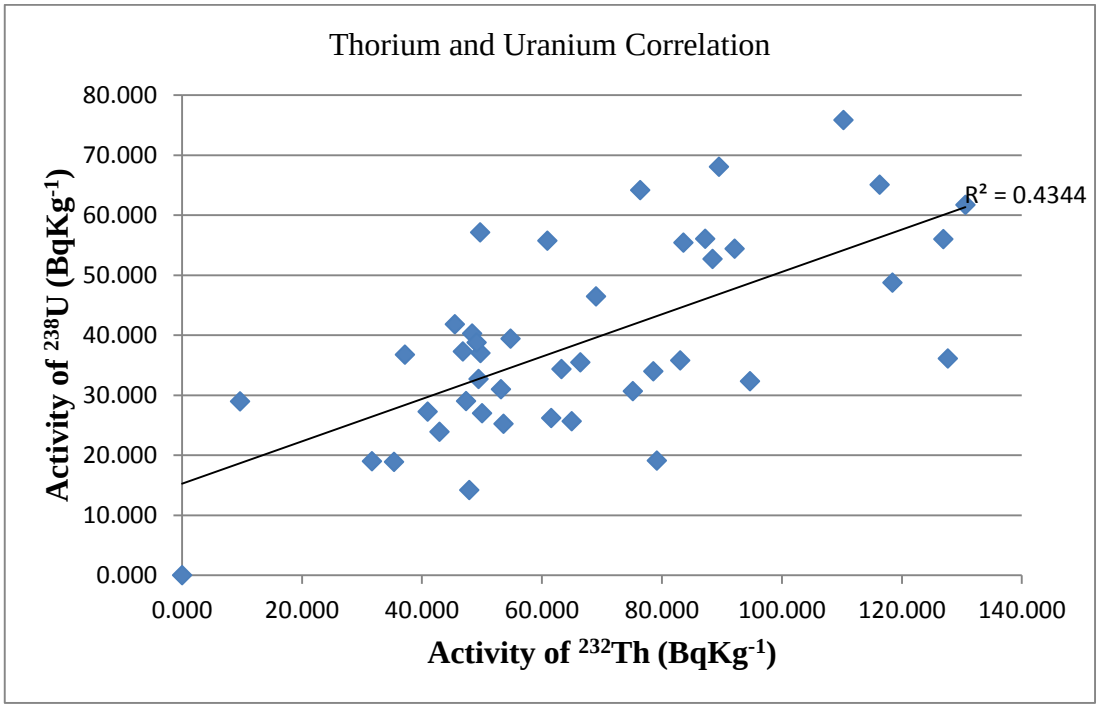

Figure 5-8: The relationship between ^{238}U and ^{232}Th activity

In general, the radionuclide activity levels in the Mui Basin is intermediate when compared to other areas that have the following minerals; biotite gneisses, migmatites, meta-granite, granitoid gneisses, quartzites, pegmatites, sillimanite gneisses and schists. The high potassium concentrations can be attributed to the presence of potassium bearing minerals; biotite, muscovite, orthoclase, microcline, feldspars, radioactive minerals; smectite, kaolite. (Okeyode & Ganiyu, 2009). However, this study did not evaluate mineralization of the study area.

Table 5-5 shows a comparative analysis of some of the areas in Kenya where radioactivity measurement studies have been done in the past.

Table 5-5: Comparative analysis of areas where radioactivity studies have been done in Kenya

	ACTIVITY CONCENTRATION RESULTS						
REGION	**^{232}Th**	**^{238}U**	**^{40}K**	**D ($nGyh^{-1}$)**	**AEDE ($mSvy^{-1}$)**	**H_{ex}**	**H_{in}**
Nairobi	117	75.9	1075	156	0.96	0.88	1.09
Kisii				178	0.44	1.27	1.03
Kitui (Limestone)	<DL	35.9	109				
Lambwe East (Ruri Hills)	1397	179	509	2300	5.7		
Mui Basin	70.6	40.5	928	102	0.13	0.57	0.68

The results of this study are consistent with those of another study by Mulwa, Maina & Patel (2013) in the limestone regions of Kitui which reported values below the recommended limits. The determined absorbed dose, AEDE, and external and internal hazard indices for the Mui basin (Block C) are lower than those measured in Tabaka-Kisii, Ruri hills-Lambwe East and Nairobi.

6.

CONCLUSION AND RECOMMENDATIONS

6.1. Introduction

From the results of measurements in this study, baseline environmental radiological assessment of the Mui Basin Block C prior to mining activities has been established. The results of this study will facilitate future monitoring of natural radionuclides in the terrestrial environment. Recommendations to mitigate impacts have been proposed

6.2. Conclusion

The study has been successful in determining the radionuclide content of naturally occurring radionuclides.in the soils of the Block C of the Mui Basin and their distribution 40K was found to be the most abundant t radionuclide followed by ^{232}Th. The radionuclide activity concentrations, gamma absorbed dose rates, annual effective dose rates were found to be all above the world average values but below the recommended ICRP limits

Generally, the external radiation hazard index from all soil samples analyzed were below unity. The radium equivalent was found to be below the 370Bqkg^{-1} world average value. There is a strong correlation (R^2=0.7597) between ^{232}Th activity concentration and the absorbed dose in the samples analyzed.

There is a weak correlation between the internuclide activities of analyzed soil samples.

It can be expected that the radiation levels and air particulates in the ambient atmosphere may increase following the commencement of mining activities, will more likely be a source of concern. Currently the radiation levels in the Block C of the Mui Basin do not pose any radiation exposure hazard risks.

6.3. Recommendations

1) Continuous and periodic monitoring of environmental radioactivity;
2) Initiate epidemiological studies to relate the environmental radioactivity to diseases;
3) To measure the ambient atmosphere absorbed and annual effective dose;
4) Analyze radioactivity in water sources; rivers, boreholes, etc.

REFERENCES

Ahmad, N., Khatibeh, A. J. A. H., Ma'ly, A., & Kenawy, M. A. (1997). Measurement of natural radioactivity in Jordanian sand. *Radiation measurements*, *28*(1), 341-344.

Ahmed, N.K., El-Arabi A.M (2005) "Natural radioactivity in farm soil and phosphate fertilizer and its environmental implications in Qena governorate, Upper Egypt", *Journal of Environmental Radioactivity* 84, 51-64.

Akiba, S. (2000). Cancer Risk in HBRAs in Yangjiang, China, and in Karunagappally, India. *Department of Public Health, Kagoshima University Faculty of Medicine Sakuragaoka 8-35-1, Kagoshima, Japan*. P-2a-S2

Al Safarjalani, A. M., Al-Dakheel, Y., & El Mahmoudi, A. S. (2007). RADIONUCLIDE LEVELS IN SOIL OF AL Hassa, KSA.

Baranwal, V. C., Sharma, S. P., Sengupta, D., Sandilya, M. K., Bhaumik, B. K., Guin, R., & Saha, S. K. (2006). A new high background radiation area in the geothermal region of Eastern Ghats Mobile Belt (EGMB) of Orissa, India. *Radiation measurements*, 41(5), 602-610.

Beir, V. I. I. (2006). Health risks from exposure to low levels of ionizing radiation. *BEIR VII phase*, *2*.

Boreham D, A Brooks, D J Higson, Y-C Luan, R E Mitchel, J Strzelczyk, P Sykes (2006). Effects of Low Doses of Radiation: Joint statement at the 15th Pacific Basin Nuclear Conference, Sydney, Australia, October 2006. Pacific Nuclear Council.

Cengiz, M., Gurkaynak, M., Vural, H., Aksoy, N., Cengiz, B., Yildiz, F., & Atahan, I. L. (2002). Tissue trace element change after total body irradiation. *Nephron. Experimental nephrology*, *94*(1), e12-6.

Chatterjee, J., Mukherjee, B. B., De, K., Das, A. K., & Basu, S. K. (1994). Trace metal levels of X-ray technicians' blood and hair. *Biological trace element research*, *46*(3), 211-227.

Cuttler, J. M., & Pollycove, M. (2009). Nuclear energy and health: and the benefits of low-dose radiation hormesis. *Dose-Response*, **7**(1), 52-89.

Das B. (2010). Genetic studies on human population residing in High Level Natural Radiation Areas of Kerala coast. BARC Newsletter, 28-37.

Ebrahiminia, A., Shahbazi-Gahrouei, D., Karegar, A., & Farzan, A. (2008). Relationship between occupational exposure and concentration of some trace elements in radiology and radiotherapy workers. *The Journal of Qazvin University of Medical Sciences*, *12*(3), 52-57.

Farai, I. P., & Jibiri, N. N. (2000). Baseline studies of terrestrial outdoor gamma dose rate levels in Nigeria. *Radiation Protection Dosimetry*, ***88*(3)**, 247-254.

Florou, H., & Kritidis, P. (1992). Gamma radiation measurements and dose rate in the coastal areas of a volcanic island, Aegean Sea, Greece. *Radiation Protection Dosimetry*, *45*(1-4), 277-279.

Freitas, A. C., & Alencar, A. S. (2004). Gamma dose rates and distribution of natural radionuclides in sand beaches—Ilha Grande, Southeastern Brazil. *Journal of environmental radioactivity*, *75*(2), 211-223.

Frissel M.J. (1994). The bioavailability of deposited artificial radionuclide: a study of the international union of radioecology working group of soil to plant transfer. Gro. Chem. Int 39:91-102

Fujinami N, Koga T. and Morishima H (nd). External Exposure Rates from Terrestrial Radiation at Guarapari and Meaipe in Brazil. P-1a-19

Gahrouei, D. S. (2003). Possible effect of background radiation on cancer incidence in Chaharmahal and Bakhtiari province. Iran. J. Radiat. Res, 1(3), 171-174.

Gesell, T. F., & Prichard, H. M. (1975). The technologically enhanced natural radiation environment. *Health Physics*, *28*(4), 361-366.

Ghiassi-Nejad, M., Mortazavi, S. M. J., Cameron, J. R., Niroomand-Rad, A., & Karam, P. A. (2002). Very high background radiation areas of Ramsar, Iran: preliminary biological studies. *Health Physics*, *82*(1), 87-93.

Harb, S., Salahel Din, K., & Abbady, A. (2009). Study of efficiency calibrations of HPGe detectors for radioactivity measurements of environmental samples.

Housheya, O. J. (2012). Measurements of the Environmental Natural Radiation in the Northern WestBank Governorate of Jenin-Palestine. Journal of Science, 2(1), 91-95.

IAEA (2003), Extent of Environmental Contamination by Naturally Occurring Radioactive Material (NORM) and Technological Options for Mitigation, Technical Reports Series No. 419, STI/DOC/010/419 (ISBN: 9201125038)

IAEA, (2002). Natural and induced radioactivity in food. Vol. 1287. Vienna: International Atomic Energy Agency.

Kannan, V., Rajan, M. P., Iyengar, M. A. R., & Ramesh, R. (2002). Distribution of natural and anthropogenic radionuclides in soil and beach sand samples of Kalpakkam (India) using hyper pure germanium (HPGe) gamma ray spectrometry. *Applied Radiation and isotopes*, *57*(1), 109-119.

Karam, P. A. (2002). The high background radiation area in Ramsar Iran: geology, norm, biology, LNT, and possible regulatory fun. *WM*, *2*, 24-28.

Karangelos D J, Petropoulos N P, Ananostakis M J, Hinis E P And Simopoulos S E (2004). Radiological Characteristics And Investigations Of The Radioactive Equilibrium In The Ashes Produced In Lignite Fired Power Plants. J. Environ. Radioact, 77; 233-246.

Kebwaro, J. M., Rathore, I. V. S., Hashim, N. O., & Mustapha, A. O. (2011). Radiometric assessment of natural radioactivity levels around Mrima Hill, Kenya. *Int. J. Phy. Sci*, *6*(13), 3105-3110.

Khandaker, M. U. (2011). High purity germanium detector in gamma-ray spectrometry. *International Journal of Fundamental Physical Sciences*, *1*(2).

Kinyua, R., Atambo, V.O. and Ongeri, R.M., (2011). Activity concentrations of 40 K, 232 Th, 226 Ra and radiation exposure levels in the Tabaka soapstone quarries of the Kisii Region, Kenya. *African Journal of Environmental Science and Technology*, *5*(9), pp.682-688.

Lebecka, J., Skubacz, K., Chalupnik, S., Tomza, I., Pluta, J., & Skowronek, J. (1987). Influence of mining activity on distribution of radium in the natural environment.

Lindell, B., & Dobson, R. L. (1961). *Ionizing radiation and health* (No. 6). World Health Organization.

Mohankumari, T. L., Anandaram, B. N., & Shilpa, G. M. (2014). A Study of Outdoor and Indoor Environmental Gamma Radiation Level in and Around Sagara and Soraba Taluk, Shimoga,

Karnataka, India. International Journal of Engineering Science Invention Research & Development; Vol. I Issue V November 2014

Mohantya A.K, Senguptaa D., Dasb S.K., V. Vijayanc, S.K. Sahab (2004). Natural Radioactivity in the Newly Discovered High Background Radiation Area on the Eastern Coast Of Orissa, India. *Radiation Measurements* **38** (2004), 153 – 165.

Mukherjee, S. P., & Vesmawala, G. (2013) Exploring Fly Ash Utilization in Construction of Highways in India. *IOSR Journal of Mechanical and Civil Engineering (IOSR-JMCE) e-ISSN: 2278-1684, p-ISSN: 2320-334X, Volume 8, Issue 4 (Sep. - Oct. 2013), PP 23-32 www.iosrjournals.org*

Mulwa, B. M., Maina, D. M., & Patel, J. P. (2013). Radiological Analysis of Suitability of Kitui South Limestone for use as Building Material. International Journal of Fundamental Physical Sciences, 3(2).

Mustapha, A. O., Narayana, D. G. S., Patel, J. P., & Otwoma, D. (1997). Natural radioactivity in some building materials in Kenya and the contributions to the indoor external doses. *Radiation protection dosimetry*, ***71***(1), 65-69.

Muthangya, M., & Samoei, D. (2006). Status of Water Quality in the Coal Rich Mui Basin on Kitui County, Kenya. ARPN Journal of Earth Sciences Vol. 1, No. 2, November 2012

Nada, A. (2003). Evaluation of natural radionuclides at Um-Greifat area, eastern desert of Egypt. Applied Radiation and isotopes, 58(2), 275-280.

Okedeyi A.S, Gbadebo A.M, Arowolo T.A, Mustapha A.O(2012) Measurement of Gamma Radioactivity Level In Bedrocks And Soils Of Quarry Sites In Ogun State, South- Western Nigeria. Research Journal of Physics 6(2): 59-65.

Okeyode I.C. and Ganiyu S.A. (2009). Measurement of Activity Concentrations of Natural Radionuclides In The Top Soil Of University Of Agriculture, Abeokuta, (Unaab) Farms Journal of Natural Sciences, Engineering and Technology

Olarinoye I.O, Sharifat A.N, Baba Kutiga M.T, Kolo and Aladeniyi K (2010). Measurement of Background Gamma Radiation Level at Two Tertiary Institutions in Minna, Nigeria.J.Appl. Science Environ. Manage, 14:59-62.

Patel, J. P. (1991). Environmental radiation survey of the area of high natural radioactivity of Mrima hill of Kenya.

Petropoulos, N. P., Anagnostakis, M. J., & Simopoulos, S. E. (2002). Photon attenuation, natural radioactivity content and radon exhalation rate of building materials. *Journal of Environmental Radioactivity*, *61*(3), 257-269.

International Commission on Radiological Protection, 1991. *ICRP Publication 60: 1990 Recommendations of the International Commission on Radiological Protection* (No. 60). Elsevier Health Sciences.

Radhakrishna, A. P., Somashekarappa, H. M., Narayana, Y., & Siddappa, K. (1993). A new natural background radiation area on the southwest coast of India. *Health Physics*, *65*(4), 390-395.

Ramachandran, T. V. (2011). Background radiation, people and the environment. *Iran J Radiat Res*, *9*(2), 63-76.

Ramli A T, Apriantoro N H, Wagiran H, Wood A K, Kuan L S (2009) Health Risk Implication Of High Background Radiation Dose Rate In Kampong, Sungai Durian Kinta District, and Perak Malaysia. *Global Journal of Health Science* **vol. 2** 2009

Ruhl, L., Vengosh, A., Dwyer, G. S., Hsu-Kim, H., Deonarine, A., Bergin, M., & Kravchenko, J. (2009). Survey of the potential environmental and health impacts in the immediate aftermath of the coal ash spill in Kingston, Tennessee. *Environmental Science & Technology*, *43*(16), 6326-6333.

Saleh L.H, Hafez A. F, Elanany N H, Motaneh H A And Naim M A (2007). Radiological Study of Soil Food Stuff and Fertilizers in the Alexandria Region. Egypt. Turk .J. Eng. Environ. Science, 31:9-17.

Senapati, M. R. (2011). Fly ash from thermal power plants- waste management and overview. *Current Science (Bangalore)*, *100*(12), 1791-1794.

Shahbazi-Gahrouei, D., & Abdolahi, M. (2012). The correlation between high background radiation and blood level of the trace elements (copper, zinc, iron and magnesium) in workers of Mahallat's hot springs. *Advanced biomedical research*, *1*.

Shamshad, A., Fulekar, M. H., & Bhawana, P. (2012). Impact of coal based thermal power plant on environment and its mitigation measure. *International Research Journal of Environment Sciences*, *1*(4), 60-64.

Shanthi G., Maniyan C. G., Allan Gnana Raj G. and J. Thampi Thanka Kumaran (2009). Radioactivity in food crops from high background radiation area in southwest India CURRENT SCIENCE, VOL. 97, NO. 9, 10 NOVEMBER 2009

Skubacz, K., Lebecka, J., Chalupnik, S., & Wysocka, M. (1992). Possible changes in radiation background of the natural environment caused by coal mine activity. *Energy sources*, *14*(2), 149-153.

Śleziak, M., Petryka, L., & Zych, M. (2010). Natural radioactivity of soil and sediment samples collected from postindustrial area.

Sohrabi, M. (1990). Recent radiological studies of high natural radiation areas of Ramsar.

Tao Z, Cha Y, Sun Q. (1999).Cancer mortality in high background radiation area of Yangjiang, China, 1979-1995. Zhonghua Yi Xue Za Zhi.; 79(7):487-92, 1999.

Tao Z, Zha Y, Akiba S, Sun Q, Zou J, Li J, Liu Y, Kato H, Sugahara T, Wei L.(2000). Cancer mortality in the high background radiation areas of Yangjiang, China during the period between 1979 and 1995. J Radiat Res (Tokyo). 41 Suppl:31-41,

Tenge, J.M., Jumba, I.O., Kariuki, D.K. and Riaroh, D.O. (2013), An Investigation to Establish the Presence, Quality and Rank of Coal from Parts of Mui Basin in Kenya. University of Nairobi Repository

Tomza, I., & Lebecka, J. (1981). Radium-bearing waters in coal mines: occurrence, methods of measurement and radiation hazard. In Radiation hazards in mining: control, measurement, and medical aspects.

Toshiyasu Iwasaki (2009). Trying to elucidate the Effects of Low Dose Radiation-From the Results of Epidemiological Studies on High Background Radiation Areas- January 2009 Central Research Institute of Electric Power Industry Public Communications Group 1-6-1 Ohtemachi, Chiyoda-ku, Tokyo 100-8126 JAPAN

Turhan S and Gunduz L (2007).Determination Of Specific Activity of Ra-226, Th-232 and K-40 for Assessment of Radiation Hazards from Turkish Pumice Samples. J. Environ. Radioact, 99:332-342.

United Nations Scientific Committee on the Effects of Atomic Radiation. (1993). Sources and effects of ionizing radiation. *UNSCEAR 1993 Report to the General Assembly, with Scientific Annexes*.

UNSCEAR 2000.Sources and Effects of Ionizing Radiation. Report To the General Assembly with Scientific Annexes Vol. 1 Source United Nations Scientific Committee on the Effects of Radiations

United Nations Scientific Committee on the Effects of Atomic Radiation, (2011). UNSCEAR 2008 report Vol. II. *Effects of ionizing radiation. Annex D: Health effects due to radiation from the Chernobyl accident (United Nations, New York, 2011)*.

Vatalis, K. I., & Kaliampakos, D. C. (2006). An overall index of environmental quality in coal mining areas and energy facilities. Environmental management, 38(6), 1031-1045.

Wakeford, R., Kendall, G. M., & Little, M. P. (2009). The proportion of childhood leukemia incidence in Great Britain that may be caused by natural background ionizing radiation. Leukemia, 23(4), 770-776.

Walter, David J.M and Glen S. (2006). Modern Nuclear Chemistry. John Wiley and Sons Hoboken New Jersey

Xhixha, G., Bezzon, G.P., Broggini, C., Buso, G.P., Caciolli, A., Callegari, I., De Bianchi, S., Fiorentini, G., Guastaldi, E., Xhixha, M.K. and Mantovani, F., (2013). The worldwide NORM production and a fully automated gamma-ray spectrometer for their characterization. *Journal of Radioanalytical and Nuclear Chemistry*, *295*(1), pp.445-457.

Životić, D., Gržetić, I., Lorenz, H., & Simić, V. (2008). U and Th in some brown coals of Serbia and Montenegro and their environmental impact. Environmental Science and Pollution Research, 15(2), 155-161.

APPENDICES

Appendix A-1 Sampling Coordinates

Location	Sample ID	Eastings	Northings
Yoonye			
	S1	411937	9870149
	S2	412571	9870325
	S3	412172	9870964
	S4	412669	9871685
	S5	413146	9872309
	S6	413173	9872110
	S8	413236	9871079
	S9	412425	9873609
	S10	412433	9875023
	S11	412176	9875697
	S12	412626	9877291
	S13	412501	9877256
	S26	413999	9879692
	S27	414403	9879634
	S28	413998	9879651
	S29	413014	9873803
	S30	414594	9879621
	S31	414028	9878767
	S32	414037	9878742
	S33	412201	9872306

Kateiko			
	S14	410966	9878310
	S15	410955	9878380
	S16	410959	9878334
	S17	419998	9879503
	S18	410438	9879787
	S19	412934	9879679
	S20	412895	9879704
	S21	414243	9880162
	S22	413969	9883132
	S23	410112	9881053
	S24	412197	9879811
	S25	414727	9880525
Kathonzweni			
	S34	412242	9872324
	S35	411632	9872552
	S36	412009	9872311
	S37	411767	9874605
	S38	412035	9875912
	S39	409946	9877261
	S40	409917	9877261
	S41	412446	9881234
	S42	410549	9883734
	S43	412035	9875912

Appendix A-2: Activity concentration of ^{232}Th, ^{238}U, ^{40}K in $Bqkg^{-1}$

ACTIVITY CONCENTRATION RESULTS			
Sample	^{232}Th	^{238}U	^{40}K
SN1	49.8 ±3.7	37.0 ±2.5	349 ±18
SN2	47.3 ±3.5	29.0 ±1.1	358 ±16
SN3	50.0 ±1.2	27.0 ±2.6	699 ±19
SN4	48.4 ±3.8	40.3 ±2.6	816 ±22
SN5	83.1 ±9	35.8 ±2.6	1519 ±23
SN6	61.5 ±4.9	26.2 ±3.3	1335 ±29
SN8	69.0 ±6.2	46.5 ±4.1	1299 ±46
SN9	31.7 ±4.9	19.0 ±2.7	686 ±23
SN10	45.5 ±3.6	41.8 ±2.5	423 ±20
SN11	127 ±6	36.1 ±5.2	810 ±33
SN12	49.4 ±6	32.7 ±3.7	1516 ±43
SN13	60.9 ±9.5	55.7 ±5.8	1247 ±51
SN14	42.9 ±7.2	23.9 ±5.9	506 ±35
SN15	35.4 ±5.5	18.9 ±3.6	412 ±25
SN16	9.7 ±5.6	29.0 ±3.7	846 ±34
SN17	79.1 ±6.9	19.1 ±4.8	583 ±28
SN18	66.4 ±4.5	35.5 ±3.1	1328 ±36
SN19	53.2 ±1.0	31.0 ±2.7	977 ±30
SN20	65.0 ±6.3	25.7 ±3.7	879 ±39
SN21	76.4 ±4.1	64.2 ±4.3	997 ±24
SN22	131 ±5.3	61.7 ±3.7	1204 ±27
SN23	110 ±4.3	75.9 ±4.2	845 ±24
SN24	49.7 ±4.8	57.2 ±7.6	1497 ±31
SN25	83.6 ±6.4	55.4 ±5.7	696 ±37
SN26	75.2 ±8.7	30.7 ±5.7	1165 ±42
SN27	92.1 ±9.7	54.4 ±6.1	1678 ±74
SN28	116 ±5	65.1 ±3.6	1622 ±35
SN29	40.9 ±7.7	27.3 ±5.4	1507 ±54
SN30	78.5 ±7.2	34.0 ±4.9	1446 ±42
SN31	88.4 ±4.5	52.7 ±2.9	1454 ±29
SN32	94.7 ±8.5	32.3 ±5.1	1498 ±42
SN33	63.3 ±5.1	34.4 ±3.9	1050 ±30
SN34	89.5 ±5.0	68.1 ±3.5	1179 ±26
SN35	37.2 ±4.0	36.8 ±3.1	611 ±26
SN36	46.8 ±34.9	37.3 ±4.1	451 ±26
SN37	54.8 ±6.4	39.4 ±4.2	477 ±28

SN38	118 ±7	48.8 ±4.1	837 ±32
SN39	87.2 ±7.8	56.1 ±5.5	691 ±35
SN40	127 ±6	56.0 ±3.7	730 ±30
SN41	53.6 ±4.4	25.3 ±3.3	903 ±26
SN42	47.9 ±4.4	14.2 ±2.9	1265 ±28
SN43	49.1 ±2.9	38.8 ±2.0	472 ±16
MEAN	68.7	39.9	973
STDEV	28.6	15.1	402

Appendix A-3 Table of dose (D nGyhr^{-1}), AEDE (mSvyr^{-1}), Radium equivalent (BqKg^{-1}), internal and external hazard indices.

SAMPLE	DOSE RATE	AEDE (mSvyr^{-}	Ra_{eq} (<370Bqkg^{-}	H_{ex} (<=1)	H_{in}
SN 1	63.7	0.078	133	0.365	0.465
SN 2	59.02	0.072	122	0.336	0.414
SN 3	74.2	0.091	147	0.411	0.484
SN 4	83.8	0.103	167	0.465	0.574
SN 5	134	0.165	261	0.733	0.83
SN 6	108	0.133	208	0.586	0.657
SN8	120	0.148	236	0.662	0.787
SN 9	58.1	0.071	112	0.316	0.368
SN 10	65.9	0.081	136	0.376	0.49
SN 11	134	0.165	275	0.759	0.857
SN 12	110	0.136	209	0.594	0.683
SN 13	116	0.143	230	0.645	0.796
SN 14	60.1	0.074	121	0.335	0.4
SN 15	48.9	0.06	98.3	0.273	0.324
SN 16	54.4	0.067	1029	0.291	0.37
SN 17	85.4	0.105	173	0.478	0.53
SN 18	115	0.141	223	0.628	0.724
SN 19	89.7	0.11	175	0.492	0.576
SN 20	91.2	0.112	180	0.503	0.572
SN 21	120	0.147	243	0.675	0.849
SN 22	163	0.201	333	0.921	1.088
SN 23	141	0.174	293	0.806	1.012
SN 24	120	0.148	233	0.657	0.812
SN 25	108	0.133	224	0.617	0.767
SN 26	112	0.138	219	0.615	0.698
SN 27	155	0.19	304	0.852	0.999
SN 28	173	0.213	345	0.962	1.138
SN 29	102	0.125	191	0.545	0.619
SN 30	127	0.156	247	0.696	0.787
SN 31	142	0.175	281	0.786	0.929

SN 32	139	0.172	273	0.764	0.852
SN 33	100	0.124	198	0.555	0.648
SN 34	138	0.17	279	0.775	0.959
SN 35	66.1	0.081	133	0.37	0.469
SN 36	66.1	0.081	136	0.375	0.476
SN 37	73.4	0.09	151	0.417	0.524
SN 38	134	0.165	277	0.763	0.895
SN 39	111	0.136	229	0.632	0.784
SN 40	139	0.171	288	0.793	0.944
SN 41	84.5	0.104	165	0.463	0.531
SN 42	91.1	0.112	171	0.486	0.525
SN 43	69.2	0.085	142	0.393	0.497
MEAN	103	0.13	228	0.58	0.68
STDEV	32.7	0.04	141	0.18	0.21
Max	173	0.21	1029	0.96	1.14
Min	48.9	0.06	98.3	0.27	0.32